Review

A review on tissue-needle interaction and path planning models for bevel tip type flexible needle minimal intervention

Hafiz Muhammad Muzzammil[1,2], Yong-De Zhang[1,*], Hassan Ejaz[2], Qihang Yuan[1] and Muhammad Muddassir[2]

[1] Key Laboratory of Advanced Manufacturing and Intelligent Technology, Harbin University of Science and Technology, Harbin 150080, China

[2] Department of Mechanical and Aerospace Engineering, Air University, E-9, Islamabad, Pakistan

* **Correspondence:** Email: zhangyd@hrbust.edu.cn; 13810467303@163.com.

Abstract: A flexible needle has emerged as a crucial clinical technique in contemporary medical practices, particularly for minimally invasive interventions. Its applicability spans diverse surgical domains such as brachytherapy, cardiovascular surgery, neurosurgery and others. Notably, flexible needles find utility in biopsies requiring deep skin penetration to access infected areas. Despite its minimally invasive advantages, the precise guidance of the needle to its intended target, while avoiding damage to bones, blood vessels, organs and tissues, remains a significant challenge for researchers. Consequently, extensive research has been dedicated to enhancing the steering and accuracy of flexible needles. Here, we aim to elucidate the recent advancements, trends and perspectives in flexible needle steering models and path planning over the last 15 years. The discussed models encompass various types, including symmetric-tip needles, curved-tip needles, tendon-actuated needles, programmable needles and the innovative fracture-directed waterjet needles. Moreover, the paper offers a comprehensive analysis, comparing the trajectories followed by these needle models to attain the desired target with minimal tissue damage. By delving into these aspects, the paper contributes to a deeper understanding of the current landscape of flexible needle technology and guides future research directions in this dynamic field.

Keywords: Flexible needle; needle steering; path planning; mechanics; surgical robotics; FEM

1. Introduction

Percutaneous treatments, which require the prolonged penetration of a flexible needle through soft tissue, are indispensable in a multitude of therapeutic situations, most notably in the execution of biopsies and brachytherapy. For such flexible needles to be efficiently guided and controlled, a model must be developed that accounts for the myriad of variables that influence needle-tissue interactions. In recent years, significant progress has been achieved by scientists in the development of mathematical and analytical models specifically designed for flexible needles that are employed in biopsies and brachytherapy. In this situation, the primary obstacle is to reach the target location precisely while avoiding bones, sensitive tissues and organs. Errors of 0.2 to 2.54 mm may transpire during needle-tissue interaction; they can be predominantly ascribed to friction, needle tip rebound, tissue and needle characteristics, non-holonomic needle motion, tissue deformation and inhomogeneity and the physiological motion of organs. The presence of these elements contributes to inconsistencies between the expected and observed needle tip deflection, highlighting the intricate nature of attaining precise and regulated needle insertion during percutaneous procedures [1–4].

A flexible needle is employed for its minimal damage benefits; however, if the needle fails to reach the desired target in a single attempt, the advantages diminish, as repeated penetration into the tissue can cause damage. In more severe cases, the needle may inadvertently enter a vital organ, leading to significant injury. The design and precise control of a steerable needle have prompted the development and adaptation of numerous analytical models. Prominent among these models are the spring-based model, bicycle model, unicycle model and kinematic model [5,6]. Furthermore, in order to maximize cost-effectiveness and time efficiency, 2D and 3D simulation methods based on Finite Element Analysis (FEA) are implemented [7–9]. To verify these analytical models, experimental experiments are performed on phantom tissue, both with and without obstructions. Significantly, two well-known models, which are routinely utilized or adjusted in the context of asymmetric bevel-tip flexible needle steering, comprise a model that revolves around the kinematics of the needle [5,6], based on a non-holonomic bicycle or unicycle model. The second model is predicated on the kinematics of tissue. based on a non-holonomic bicycle or unicycle model. The second model is predicated on the kinematics of tissue [10].

Following the successful development of models for needle-tissue interaction, the formulation of an algorithm for motion and path planning becomes imperative for the controller to effectively manage the rotation and translation motion of the needle. The principal objective of motion/path planning is to determine the most practical and efficient path from the point of insertion to the target, while ensuring that any obstructions for the needle's tip are avoided. Neurons, blood arteries, organs and bones are all possible manifestations of obstacles in the human body. A multitude of algorithms have been developed in an effort to tackle this difficulty. A path planning technique that is particularly remarkable in the context of nonholonomic systems is Sample-based Rapidly-exploring Random Trees (RRT). Specifically, when compared to simple RRT, 2D RRT with cell-decomposition path points has proven to be more effective. Incorporating impediments into a limited environment, both Forward RRT and Reverse RRT have been utilized to control the needle's travel and identify its entry point [1,2]. Furthermore, a screw-based path planning approach has been devised for a 3-D environment replete with obstacles, with subsequent simulation validating the efficacy of this path planning strategy [11].

In the realm of 2D kinematic models, reversed path planning also proves to be an advantageous method. This strategic methodology not only generates an ideal route but also identifies the point of entrance and proposes a trajectory that efficiently overcomes impediments [2]. A number of other path planning methodologies have been implemented and embraced in an effort to improve outcomes. Prominent contributors to improved outcomes in needle navigation and control include Adaptive Path Following (APF), Improved Particle Swarm Optimization Algorithm (PSO), Bee-foraging Learning Particle Swarm Optimization (BFL-PSO), Inductive Learning-based and Deductive Reasoning-based (ILDR) and Breadth-First Search with Genetic Algorithm (BFS-GA) [12–16].

The effectiveness of flexible needle therapy is contingent not only on the choice of model but also on the meticulous management of various physical parameters. These parameters encompass needle deflection, the angle of the needle tip, needle buckling, phantom tissue properties and the elasticity of the needle material, among others. Failing to appropriately account for and control these factors can compromise accuracy, undermining the fundamental purpose of flexible needle theory and potentially causing harm to the tissue. Moreover, manually controlling needle translation speed and rotational angle poses significant challenges. To address this difficulty, various controlling devices have been developed to afford more precise and reliable control over the needle during therapeutic procedures.

We greatly contribute by providing a comprehensive review of various models, algorithms, experimentation and controlling devices involved in needle steering, path planning and control. This review distinguishes itself by offering an inclusive overview, a departure from traditional surveys focused solely on robots or specific needle types. To the best of our knowledge, this paper is the first to comprehensively elucidate the interplay of models, path planning, and controls for needles.

The paper's structure is organized as follows: (1) An introduction outlining the contributions of the paper, (2) a detailed exploration of the mathematical and Finite Element Method (FEM) modeling employed in the covered studies, (3) an in-depth discussion of algorithms for motion and path planning in both 2D and 3D environments, (4) an experimentation section featuring comparisons between needle designs developed by researchers and the controllers facilitating needle motion and finally, (5) a concluding section summarizing the key findings and contributions of the paper.

2. Tissue-needle interaction models for flexible needle steering

In soft tissue, the development of flexible needle steering necessitates the use of tissue-needle interaction models capable of forecasting the needle and needle tip motion in response to inputs provided at the needle's base. First time Park et al. [5] in 2005, presented a non-holonomic kinematic model to enable minimum invasive surgical intervention without any obstacles. They used the Euclidean group for formulating path planning of needle through firm tissue. Webster et al. [6] further improved the model and presented the robotic devices for steering a flexible needle using bevel tip. Later on, more accurate models were developed by incorporating additional governing factors of needle steering by various researchers [2,17–21]. The brief summary of the developed models is shown in Table 1, while discussion on these is given in the subsequent sections. By overviewing Table 1, researchers can easily understand the basic model for understanding and subsequently modification by introducing mathematical factors for some particular application. Also, in validation tasks, where model completely fits with the simulation or experimental result. Which in return can give a better

choice to select the model for needle penetration and deflection into the tissue.

Table 1. Development of needle steering models.

Sr No.	Author	Basic model	Modification	Mathematical Factors	Error (mm)
1	Park et al. (2005)[5]	--	Non-holonomic model	Lie Group notation	
2	Webster et al. (2006) [6]	Non-holonomic model	Bicycle and unicycle model	Lie algebra	1.3 mm bicycle (RMS) 2.6 mm unicycle (RMS)
3	Y.J. Zhao et al. (2012)[2]	Non-holonomic model	Modify with rebound parameters	kinematic model	
4	Zhao et al. (2014) [22]	Non-holonomic reduced-order model	Robust observer-based feedback control	Lie Group theory	
5	Khadem et al. (2017) [23]	Non-holonomic model	Reduced order model	Kinematic model	
6	Khadem et al. (2017) [24]	Reduced order model	Transform reduced order model	Frenet-serret Frame	0.91 (3rd scenario) (RMS)
7	Khadem et al. (2019) [25]	Reduced order model	Event triggered control	Theory of connections to transform	0.90 (plastisol) (RMS)
8	Zhao et al. (2019) [26]	Non-holonomic unicycle/ bicycle model	Unicycle /bicycle model with rebound	Kinematic model	0.5480 (MUMR) RMS)
9	Glozman et al. (2004) [10]	Linear beam	Virtual spring model	Quasi-static motion	Not measure
10	Yan et al. (2009) [18]	Virtual spring model	Spring-beam-damper model	Bernoulli-euler beam model	
11	Asadian et al. (2011) [20]	Mechanics-based model	Dynamic modelling with tissue, cutting, and friction forces	Euler-Bernoulli beam theory	
12	Goksel et al. (2009) [19]	DiMaio and Salcudean simulated (3-node triangular elements)	3D (4-node tetrahedral elements)	FEM	
		--	Angular spring model (needle discrete into small elements)	Quasi-static simulation	

Continued on next page

Sr No.	Author	Basic model	Modification	Mathematical Factors	Error (mm)
13	S Misra et al. (2010) [27]	--	Mechanics based model	Buckingham π theorem	0.3 (Most stiff plastisol (φ0.46)) 0.99 (least stiff plastisol (φ0.36)) (RMS)
14	Roesthuis et al. (2012) [28]	Mechanics based model	Combination of tip force, distributed load and a series of springs to model needle-tissue interaction	Rayleigh-Ritz method	Max. error 0.5
15	Mohsin Khadem (2015) [29]	Mechanics based dynamic model	Combination of tip force, effects of tissue deformation, friction, tissue cutting force, bevel angel and needle deflection	Euler-Bernoulli beam	Max. error 0.66
16	Rossa et al. (2016) [21]	Goksel's discrete model	Lumped needle model (discrete into rigid bars connected by helical springs	--	0.1143 (Gelatine)
17	Rossa et al. (2016) [30]	Cantilever beam	Quasi-static model	Rayleigh-Ritz method	0.36 (RMS)
18	Lehmann et al. (2017) [31]	Quasi-static model	Needle-tissue interaction model with lateral force	Euler–Bernoulli beam theory	Max. error 1.5
19	Watts et al. (2019)[32]	Non-holonomic model	Mechanics based steering model for PBNs	Euler–Bernoulli beam theory	0.2636 (n=4) with FEM 0.00112 with exp. (RMS)

The nonholonomic model proposed by Park [5] addresses only the unicycle basic model and lacks experimental validation. Additionally, this model was the most basic iteration of the nonholonomic unicycle model, devoid of any obstacles or living tissue. Webster's [6] nonholonomic model introduces the bi-cycle model and modifies Park's unicycle model. Trails confirmed that Webster's bi-cycle model was more dependable than the unicycle model. In 2012 and 2019, Zhao et al. [2] implemented a rebound component into the unicycle model and validated it through simulation. Xingang Zhao et al. [22] and Khadem et al. [23] modified bicycle model in 2014 and 2017 compensate tissue uncertainty into bicycle kinematic model. The initial virtual spring model was introduced by Glozman et al. [10] in 2010. Subsequent models incorporate several factors, including damper effect, helical spring and angular spring, as illustrated in Figure 1. First, the mechanics-based model [27], based on Buckingham's theorem, included variables about needle tissue interaction. Additionally, certain models based on mechanics were constructed using the Rayleigh-Ritz and Euler-Bernoulli beams

theories. Figure 1 shows complete classifications of the models and also relationships with each other. Also, Figure 1 gives a complete information about modeling parameters, type of model (whether it is 2D or 3D) and validation performed.
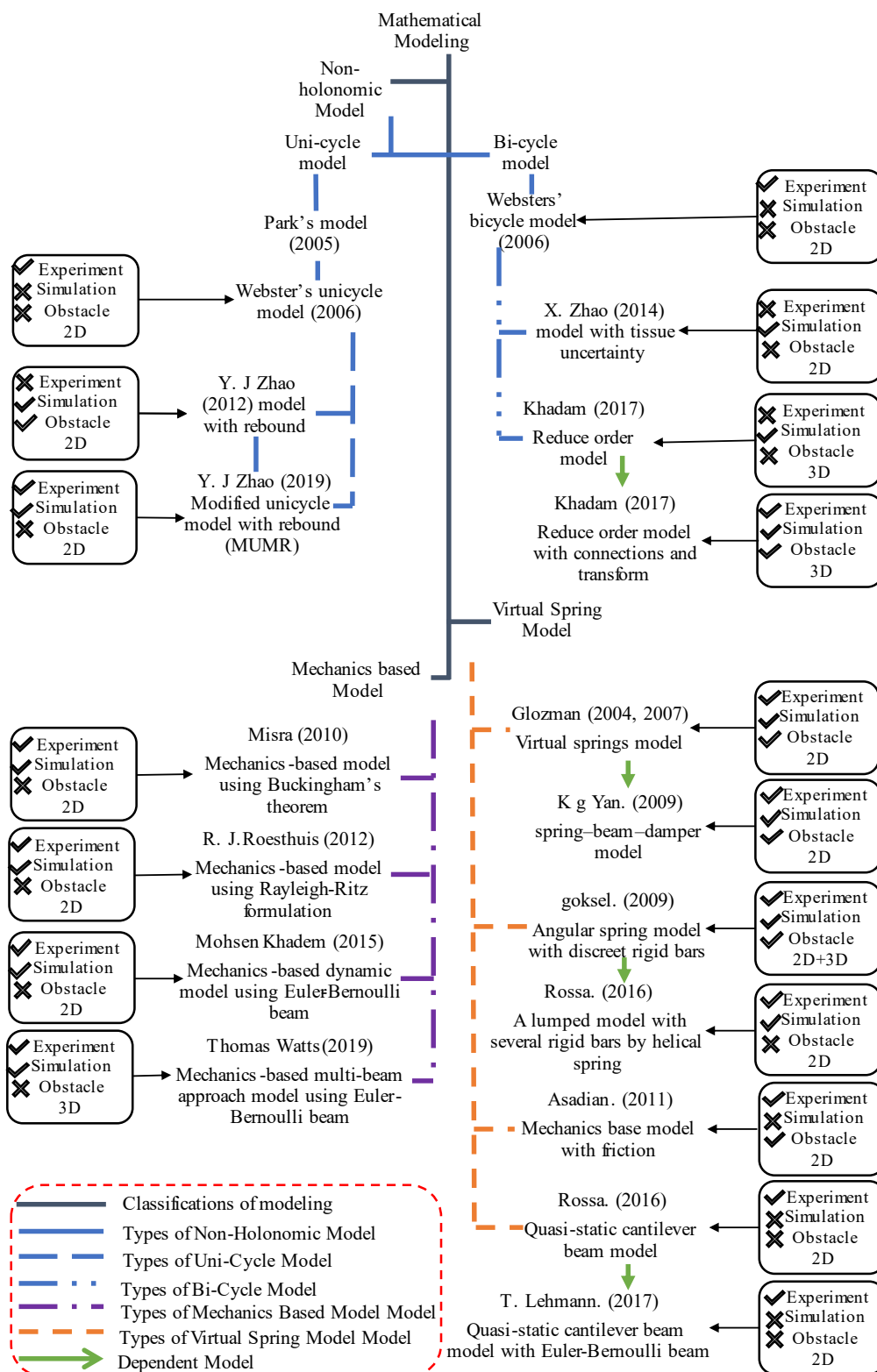

Figure 1. Comparison and relationship between all the models for flexible needle steering.

2.1. Non-holonomic model

Non-holonomic bicycle model is the most prevalent and simple model for steering the flexible needle. The model was presented by webster et al. [6], which is somehow related with diffusion-based motion planning model, and was initially presented by Park et al. [5]. The key benefit of the bicycle model is its accuracy to reach target. In contrast, the unicycle model has a greater root mean square error between the observed value and the predicted value, which in practical practice rendering bicycle model more useful. The bicycle model and unicycle model exhibit error values of 1.3 mm and 2.6 mm, respectively. Webster et al. [6] bicycle model consists of two hypothetical wheels, with fixed front wheel angle (ϕ) and the wheelbase (l_1), as shown in Figure 2. l_2 is the distance between the tip of the needle and the back wheel. Curvature of the needle shaft k is determined by the fixed front wheel angle ϕ and wheelbase l_1. One global coordinate system, denoted as A, and two local coordinate systems, denoted as B and C for the rear and front wheels, respectively. The model was represented in two dimensions for simplicity. Also, the model takes into account two input parameters: u_1, which represents the translational speed in the z direction of the local coordinate, and u_2, which denotes the rotation from the needle shaft. With a radius of $1/k$ and a curvature of k, the needle adheres to a constant circle when translation u_1 is applied. The functions of the path followed by the flexible needle in soft tissues are as follows:

$$p = f(\varphi, l_1, l_2)$$

$$p = f(r)$$

(1)

The radius of the needle arc is:

$$r = \frac{1}{k} = \sqrt{m^2 + (l \cot(\varphi))^2}$$

(2)

Bicycle model by Webster has two parameters in contrast to unicycle model. Although this results in a more intricate solution, but affords precise needle steerability in contrast to the unicycle approach [6] . The unicycle/single-wheel model is subject to two limitations in a plane: No slippage and $V_y = 0$. An angular velocity denoted as ω is a variable that functions as a control input for the unicycle model. Considering that both the needle and the tip angle are fixed in the z-direction, $V_z = r\omega = 1/k* \omega$ may be calculated. In that situation, delineate a circular trajectory for the unicycle model using the formulas for radius r and curvature k, as shown Figure 3.

The simulated trajectory predictions for both unicycle and bicycle models are illustrated in Figure 4. By applying the values $l_2 = 2\ cm$ and k = 0.05, the insertion simulation consists of the subsequent five steps: Step 1. Insert the needle for 1 second at a speed of 10 cm/s, Step 2. Rotate the needle 180 degrees, Step 3. Insert the needle for 2 seconds at a speed of 10 cm/s in, Step 4. Rotate the needle 180 degrees again, Step 5. Insert the needle for 1 second at a speed of 10 cm/s.
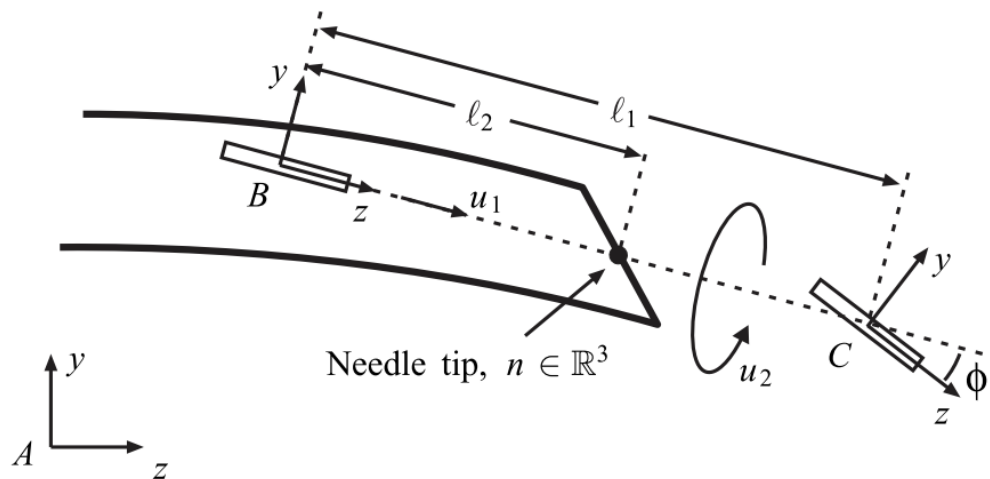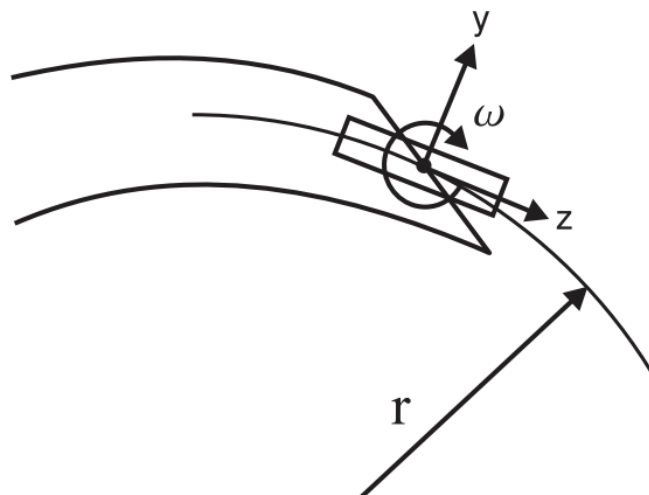
Figure 2. Non-holonomic bicycle model [6].

Figure 3. Unicycle/ single wheel model in 2D [6].

For the bicycle model, the parameters are k = 0.0449 and $l_2 = 2.3775\ cm$, with a 95% confidence level. Regarding the unicycle model, k is defined as 0.0468. Additionally, the graph demonstrates that the unicycle model has a 2.6 mm root mean square error (RMSE) between its observed data point and model forecast, whereas the bicycle model has a 1.3 mm RMSE. The bicycle model exhibits a reduced error rate, indicating enhanced reliability, though the unicycle has more straightforward formulation.

Khadem et al. [25] affixing a local coordinate frame at the needle tip and an inertial coordinate frame {O} at the needle's entry point, the current non-holonomic model was transformed from two dimensions to three. At the outset, both frames are aligned. Nevertheless, as the needle is introduced into the tissue, it adheres to a consistent curvature path K in x$'$y$'$ plane and undergoes rotation about the z$'$-axis, as illustrated in Figure 5. In addition, a nonlinear controller for 3D needle steering was developed using a non-holonomic steering model as its foundation. In order to design a two-step controller utilizing a transformed model, a reduced-order needle steering model and geometric reduction process were implemented [24,25].
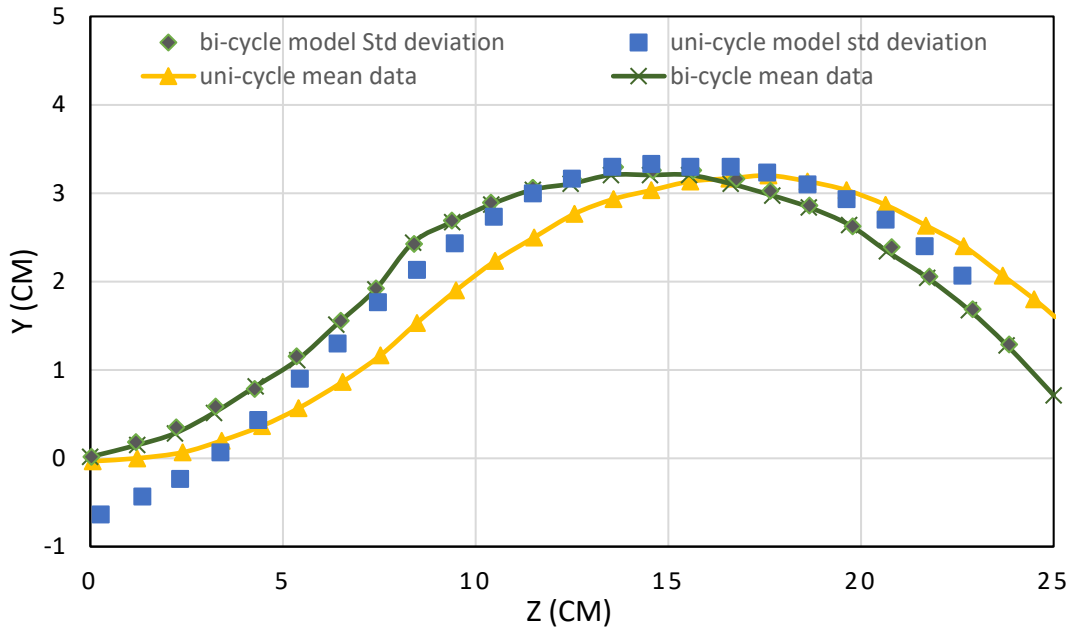
Figure 4. Unicycle and bicycle models prediction at two rational curves including average data and standard deviation.
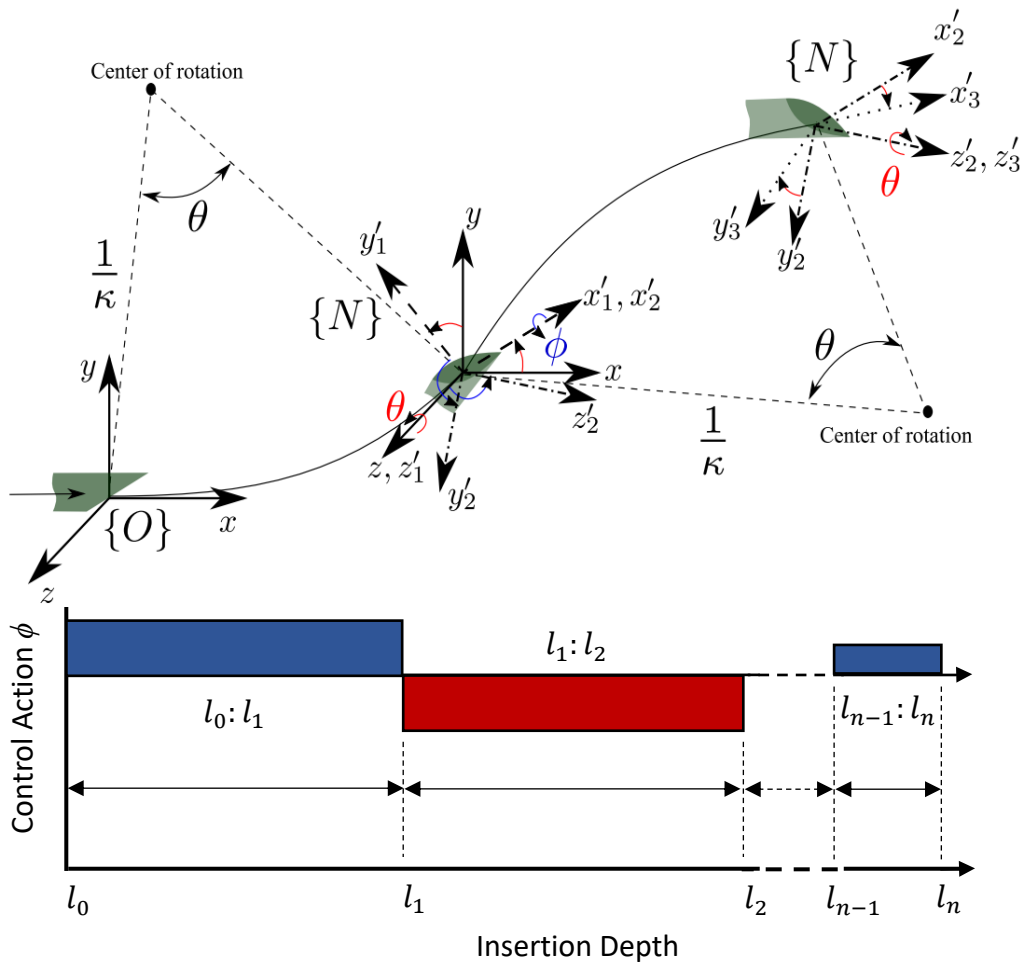

Figure 5. Schematic of reduced-order needle steering by Khadem et al. [24].

The needle encounters a rebound during reorientation at arc-arc, length-arc or arc-length due to its flexibility; this results in a significant discrepancy between the model and actual needle route [26]. To compensate for that, a modified function with rebound parameters in simple unicycle and bicycle model is added. The depiction of the modified model is shown in Figure 6.

The functions of unicycle model with modified rebound parameters are govern by equation.

$$p = f(r, b) \tag{3}$$

$$p = f(r, \varphi, b)$$
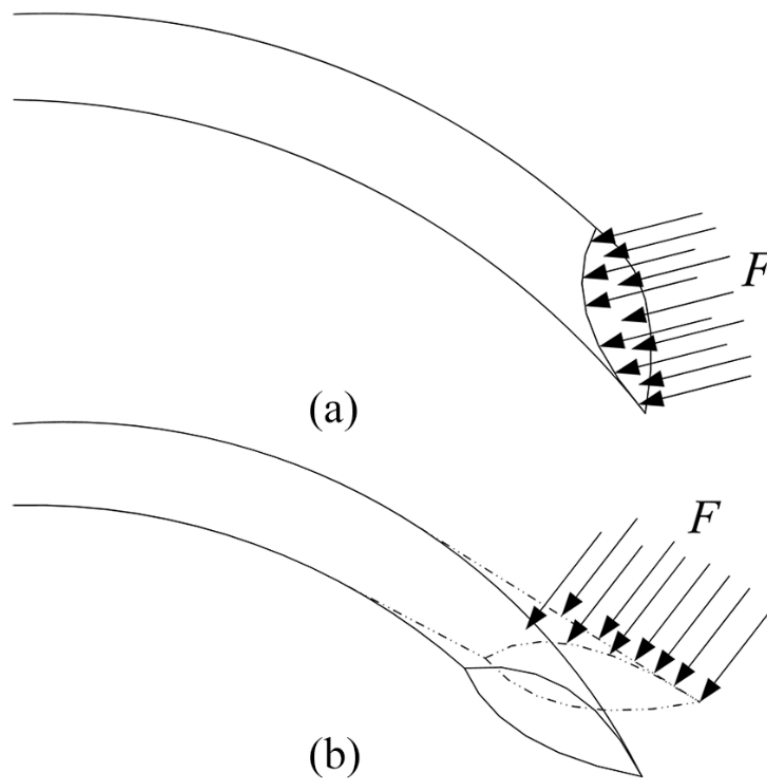
Figure 6. Effect of rebound at orientation of needle, (a) Before rotation, (b) After rotation [26].

2.2. Virtual spring model

Virtual spring modeling is predicated on the investigation of quasi-static motion, in which each needle step represents an equilibrium condition, under the assumption that biological soft tissue deflects linearly at tiny displacements. The virtual spring model incorporates two distinct types of forces: Tissue forces, which are represented as tangential friction forces along the needle shaft and lateral virtual spring forces at needle curvature, as seen in Figure 7 [10].

On the basis of the assumption that soft tissue causes a small deflection and shows linear behavior, Glozman el al. [10] modeled the needle as a linear beam to point forces with suitable element spacing (Figure 8). This assumption represents a flexible beam just like in an elastic foundation model.

At each node, the virtual spring force is proportional to the spring displacement from initial position:

$$F_i = k_i(w_i - w_{0i}) \tag{4}$$

Here, k_i spring coefficient, w_i is displacement of spring at i position, and w_{0i} shows position of free spring at i position
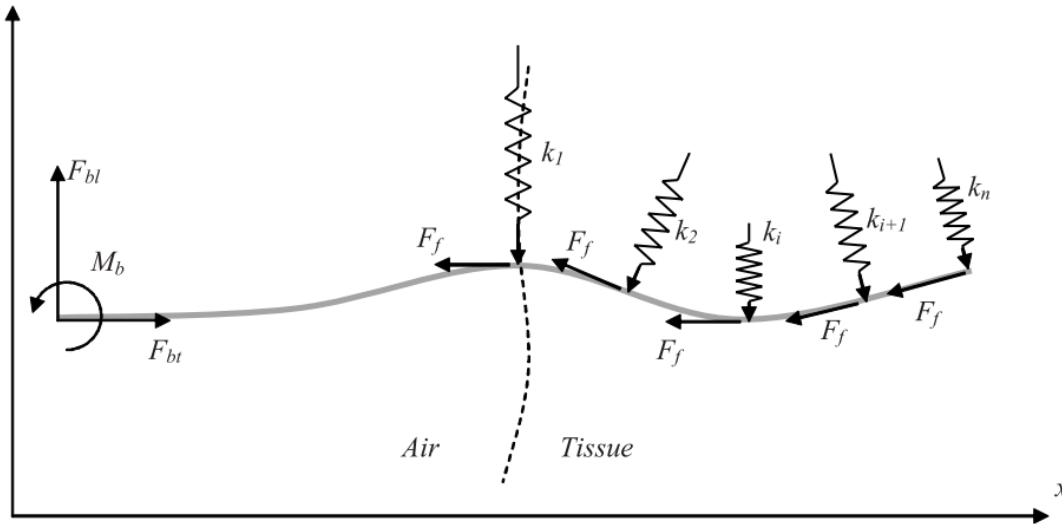

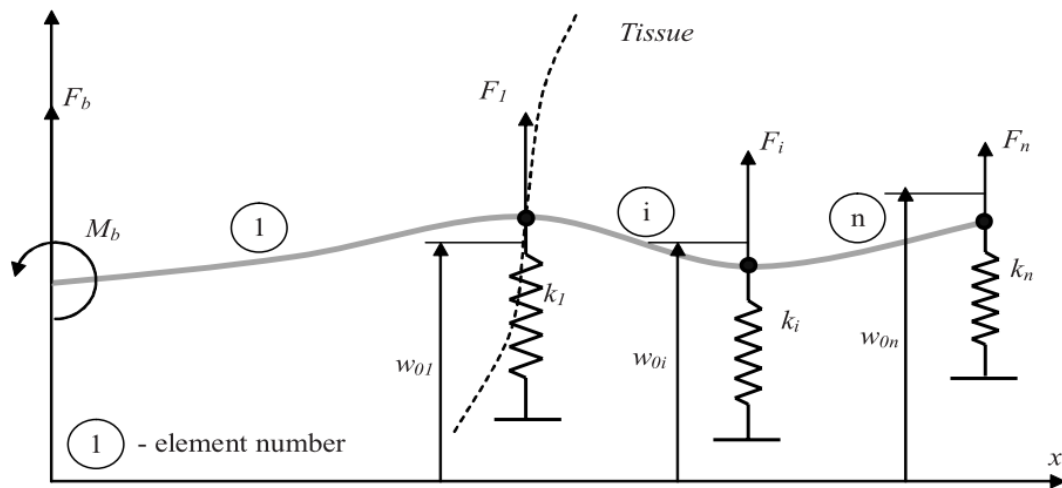**Figure 7.** Virtual spring model [10].

Figure 8. Flexible beam model [10].

In 2007, Glozman et al. [33] extend their virtual spring model with real-time fluoroscopic guidance using an inverse-forward kinematics algorithm in 2D animal tissues. Yan et al. [18] in 2009 extended the Golzman el al. [10] virtual spring model to spring beam-damper model. They proposed damper dynamics during needle-tissue interaction with the consideration of inhomogeneity of tissue and depth-varying mean parameters to accumulate spring and damper effects, as shown in Figure 9. Based on this approach, an online parameter estimator was developed using the modified least square method with forgetting factor.

Sadati et al. [34] used biological data taken from an experimental setup to create a realistic artificial brain tissue model using a non-homogenous spring network. By acting as a damper, the controller attenuated the disturbances. In a sense, the model is helpful because it incorporates the effects of non-homogeneity and uncertainty during needle steering. Asadian el al. [20] expanded the model based on mechanics by dynamically adding the friction distribution and tissue elasticity. They applied the theory of beam which assumes that the cross-section does not deform during deflection. The elasticity of tissue incorporated by assuming a large number of translational virtual springs around the needle act as supports to the beam. Along with the elasticity of the tissue, static friction was also incorporated in the deflection equations in needle bending model as can be seen in Figure 10.
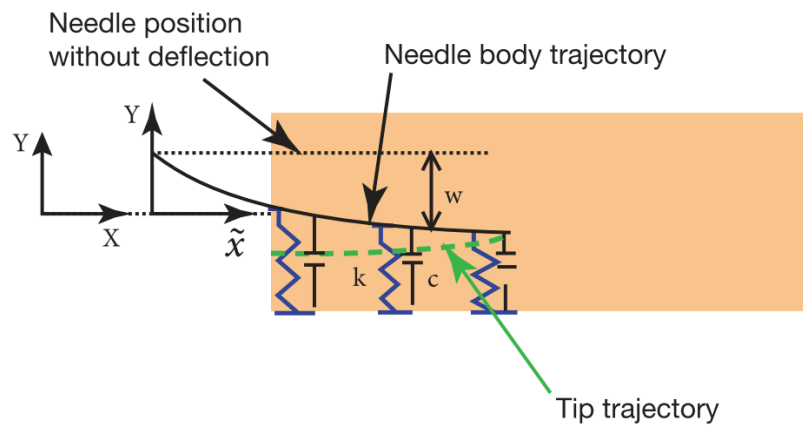
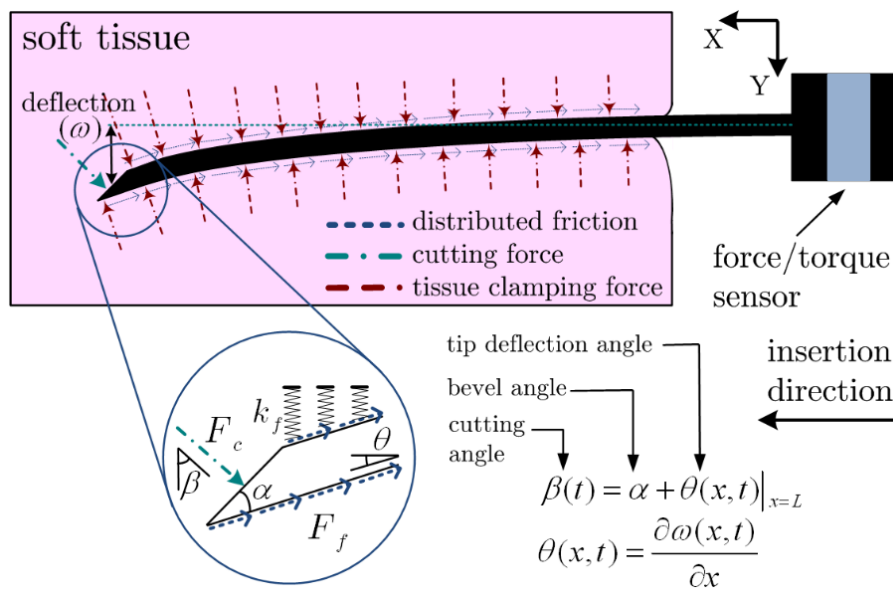**Figure 9**. Spring-beam-damper model [18].

Figure 10. Effect of cutting, friction and tissue forces on the needle [20].

Rossa et al. [30] also presented a quasi-static cantilever beam modelling of the needle in soft tissue. Compared to Yan's [18] beam model, the needle here is modelled as a vibrating beam which experiences forces applied by the surrounding tissues. The model can also compare the actual needle

position with the path cut by the needle tip in order to measure the contact force along the needle shaft as can be observed in Figure 11.

Lehmann et al. [31] extended the quasi-static model by incorporating the equations for the actuated needle acting as a cantilever beam (Figure 12). In Figure 12(a), considering a cantilever needle from point A to C, A is the fixed needle guide which is assumed as a virtual clamping. Two-point loads are applied at point B and C and tissue forces are assumed as a virtual spring along the needle insertion. The needle actuated guide applies a point force F_l at point B, which displaces needle laterally. The guide act as a fulcrum, which can be displaced in a transverse direction relative to the needle insertion axis. The needle can be pivoted about the insertion axis which results in the change in slope of the needle, as shown in Figure 12(b).
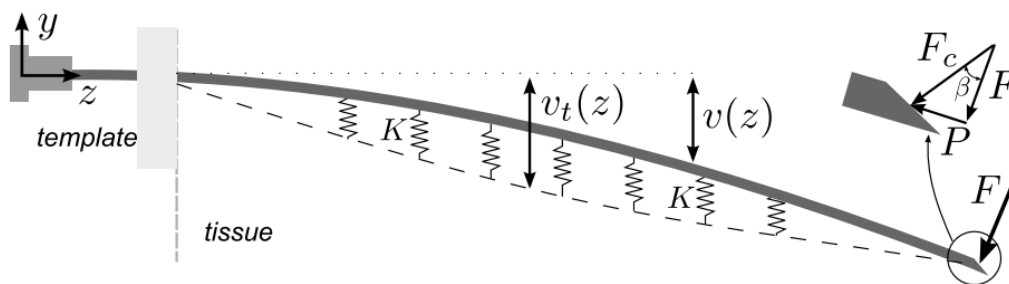

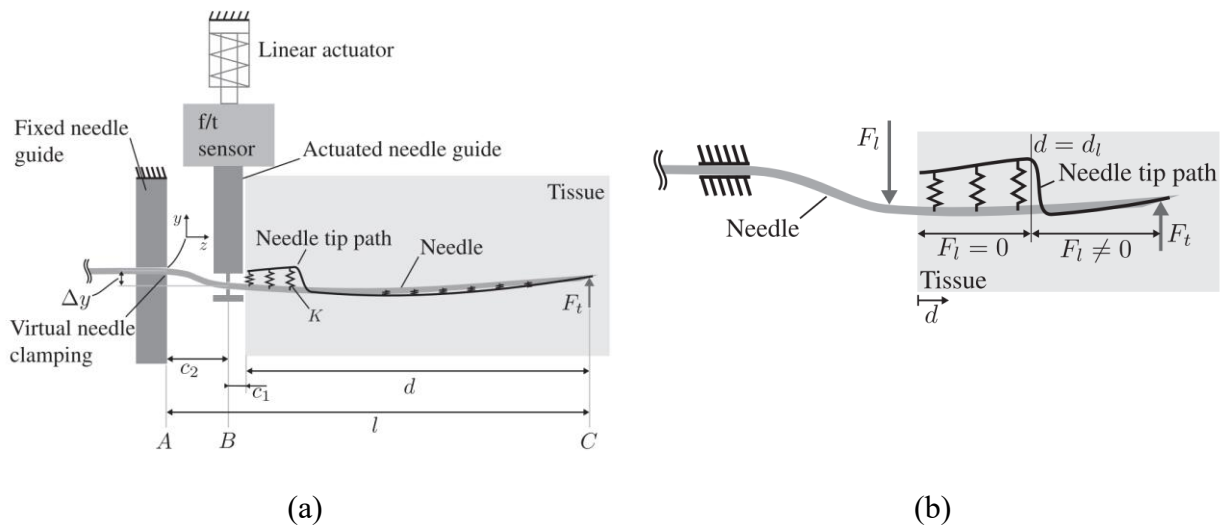**Figure 11.** Quasi-static cantilever beam [30].

(a)   (b)

Figure 12. Lehmann's needle-tissue interaction model, (a) Needle guidance at A and cutting force at C (b) A close-up view of the needle inside tissue with lateral force applied [31].

2.3. Mechanics based models

The main relationship established by mechanics-based models of the tissue-needle interaction is that of needle curvature and the material and physical characteristics of the tissue and needle. Equation 5 and Figure 13 shows, a number of factors affect the needle's radius of curvature, including

the needle material's Young's modulus (E), bevel tip angle (α), second moment of inertia (I), tissue properties exerting cutting force (F_c), coefficient of friction (F_f), needle-tissue interaction force (Fs), needle insertion velocity (V) and rebound angle (φ). Researchers have incorporated some or all of these factors into their models to capture the complexities of needle-tissue interactions.

$$\rho = f\left(E, \alpha, I, F_c, F_f, F_s, V, \varphi\right) \tag{5}$$

The equilibrium equation in the y-direction for the small element (dx) of the beam is obtained by equating the inertial forces to the sum of exerted shear forces and external loads in y-direction.

$$\rho A dx \left(\frac{d^2\omega}{dt^2}\right) = \frac{ds}{dx} dx + F_y dx \tag{6}$$

The four primary components of the mechanics-based model are as follows: Forces of tissue on the needle cylinder, tissue cutting caused by the needle tip, bending (curvature) during needle insertion and needle-template interaction, as can be seen in Figure 14 and Figure 15 respectively [29].
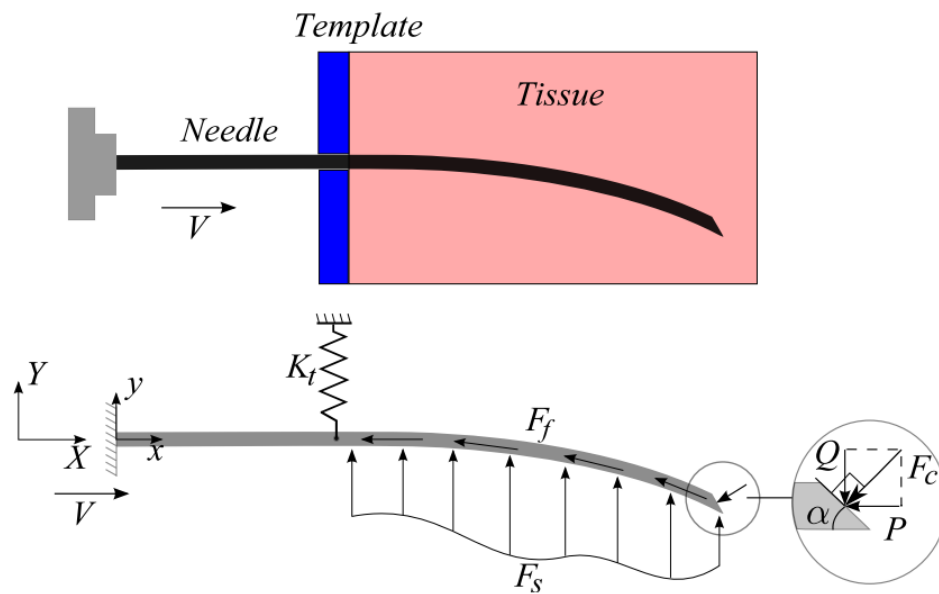

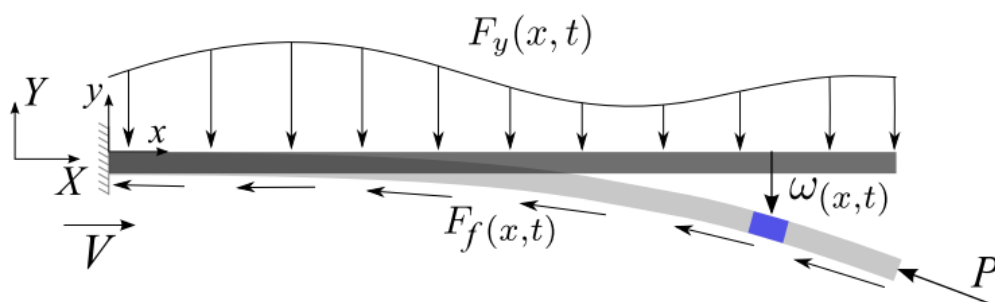**Figure 13.** Forces on tissue inserted needle [29].

Figure 14. Flexural behavior of straight beam in x-y plane under transverse and axial loads [29].
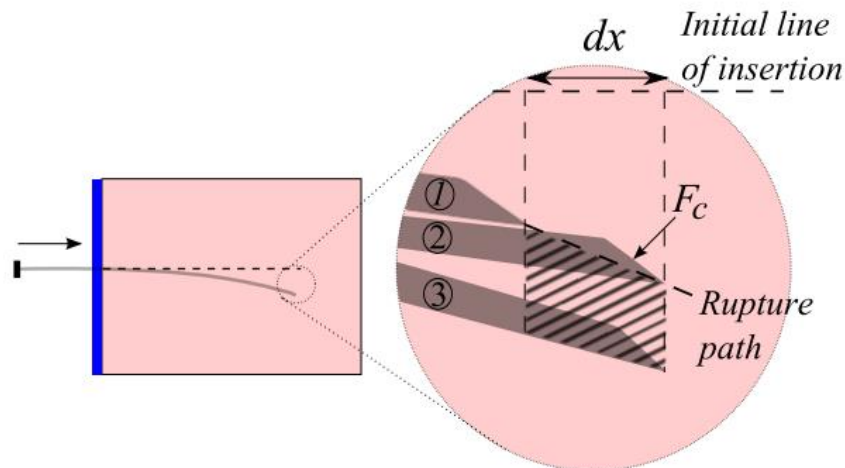
Figure 15. Schematic view of infinitesimal needle insertion: 1. Insertion point, 2. Needle penetrate through tissue, 3. Cutting force applied perpendicularly causes needle deflection [29].

Goksel et al. [19] introduced a model of an angular spring for a brachytherapy needle. In this model, a joint is produced between two segments, and the needle is made up of several rigid bars that are attached to one another. Each new part moves, bends and twists in relation to the one before it. As seen in, the needle's bending is indicated by angle θ from the x-axis and its torsion is indicated by angle α about the segment. See Figure 16 for reference.

Rossa et al. [21] proposed a lumped needle model in free space to estimate needle deflection. To propose this model, the needle is considered as a discrete structure composed of several rigid bars connected with virtual joints, as shown in Figure 17. The model is similar to the Goksel's [19] angular spring model where successive element bend relative to the previous segment; however, no rotational information is present.
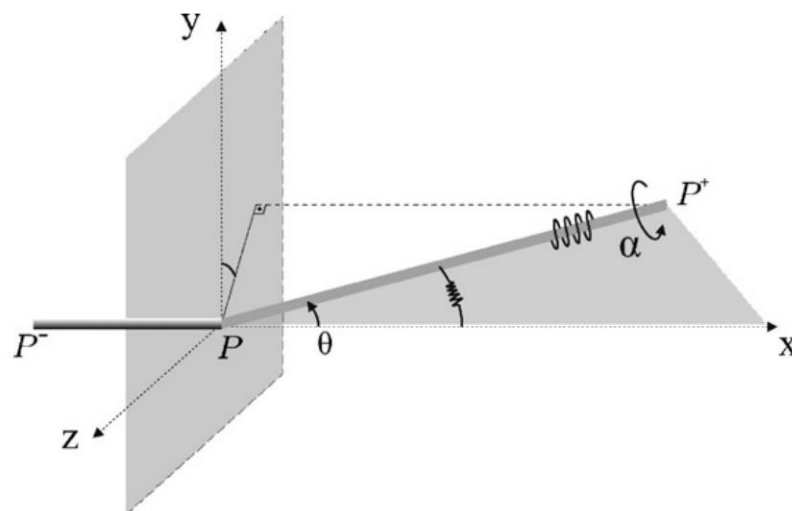

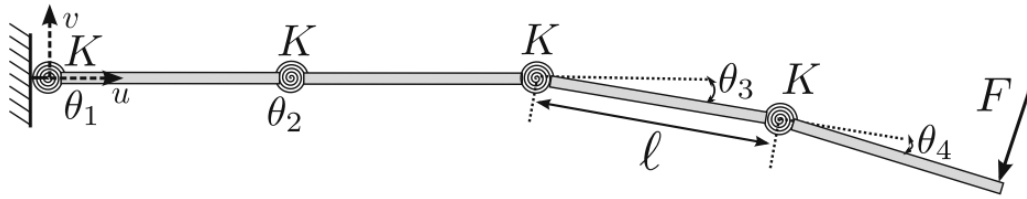**Figure 16.** Angular spring model; Bending and twisting between two segments [19].

Figure 17. Lumped model of a flexible needle [21].

2.4. Stochastic model

Both internal and exterior noises are applied to Webster's non-holonomic model. While outward noises are mostly caused by the environment, internal noises are primarily produced by sensors and actuators. Models with a stochastic foundation can make up for these mistakes. These noises are explained by a stochastic model based on the straightforward equations [5,35].

$$
\begin{aligned}
\omega(t) &= \omega_0(t) + \lambda_1 \omega_1 \\
v(t) &= v_0(t) + \lambda_2 \omega_2 \\
\omega(t) &= \omega_0(t) \\
v(t) &= v_0(t)
\end{aligned}
\tag{7}
$$

Here, $\omega_0(t)$ and $v_0(t)$ are the rotation and velocity input in ideal condition, $\omega_1(t)$ and $\omega_2(t)$ are the uncorrelated gaussian noises with λ_1 and λ_2 are the constants. Thus, non-holonomic needle model with noise is given by

$$
(g^{-1}(t)\dot{g}(t))^\vee \, dt = \begin{bmatrix} kv_0(t) & 0 & \omega_0(t) & 0 & 0 & v_0(t) \end{bmatrix}^T dt + \begin{bmatrix} 0 & 0 & \lambda_1 & 0 & 0 & 0 \\ k\lambda_2 & 0 & 0 & 0 & 0 & \lambda_2 \end{bmatrix}^T \begin{bmatrix} dW_1 \\ dW_2 \end{bmatrix}
\tag{8}
$$

This noise model is a stochastic differential equation. Webster's non-holonomic model without noises is given below:

$$
V_{xy}^b = \begin{bmatrix} v_{xy}^b \\ \omega_{xy}^b \end{bmatrix} = \left(g_{xy}^{-1} \dot{g}_{xy} \right)^\vee
\tag{9}
$$

Where $g(t)$ is the rigid body motion, k is the radius of curvature, v and ω are velocity and rotational parameters, respectively.

2.5. Finite element-based models

A mistake in needle placement may occur when the needle penetrates soft tissue and causes the tissue to shift or distort. In this situation, even a skilled surgeon treating cancer with brachytherapy or inserting seeds into patients may make an average mistake of about 6 mm [36].

The deflection of a needle in soft tissue can be planned for with the help of finite element-based simulation, or FEA. Using this method, the analytical models may be validated, which can save a lot of money and time compared to doing it experimentally. In addition to saving time and money, FEM simulations can also identify the best course for the needle insertion procedure. This path can then

serve as the basis for experimentation rather than the trial-and-error approach [1].

Alterovitz et al. [37] created a simulation based on a 2-D FEA in 2005. The scientists used a 2D finite element model to calculate tissue deformations since they assumed of tissue as a soft material with linear elastic characteristics. The steerable needle's friction forces and needle tip contact caused these deformations. Additionally, a polygon-shaped obstruction that the needle must avoid was taken into consideration. An MRI scan of the prostate (Figure 18) was used as a base for the FEA model. The model successfully reached the target by avoiding the set obstacles.
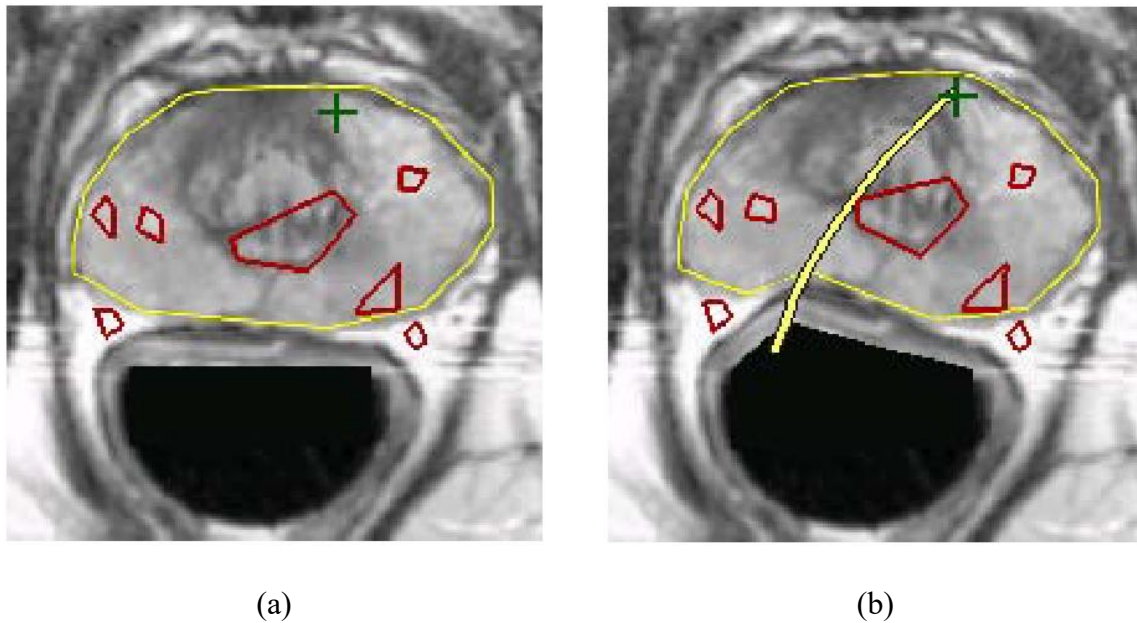

(a)   (b)

Figure 18. MRI based example for FEM simulation, (a) Red polygons present obstacles and the green cross shows target, (b) Bevel right plan [37].

Alterovitz et al. [38] improved on their earlier work by incorporating the impact of cutting forces and friction along the shaft and by displaying real-time ultrasound images of the prostate gland. The prostate glands attempted to rotate as the needle was inserted, which caused a difficulty because of the differences in stiffness between the prostate gland and the surrounding tissue (Figure 19). A physical dynamic simulation was run in order to encounter this rotation. By visualizing ultrasound pictures, the simulation adjusted the mesh surrounding the needle and modeled the impact of cutting forces and friction along the shaft in real-time.
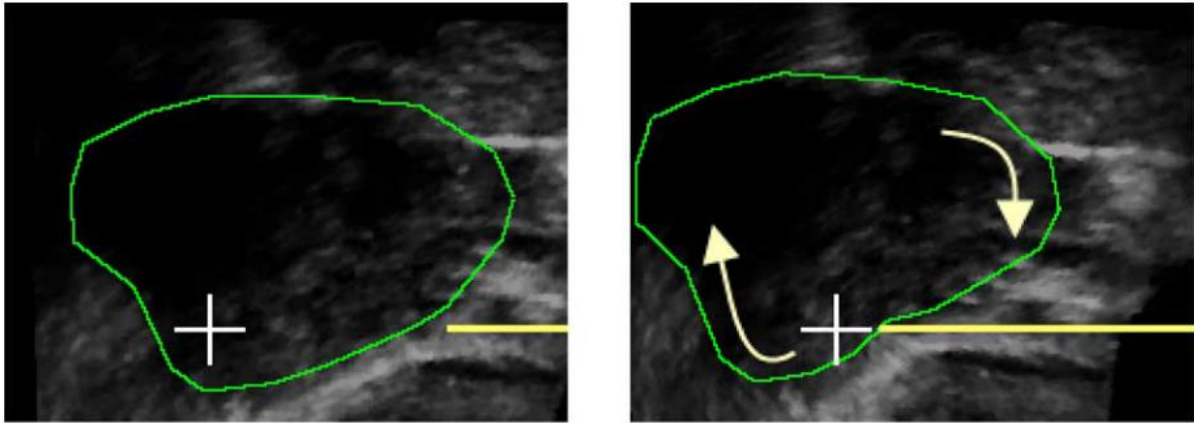
Figure 19. Rotation of the prostate gland during the insertion of the needle as experienced by [38].

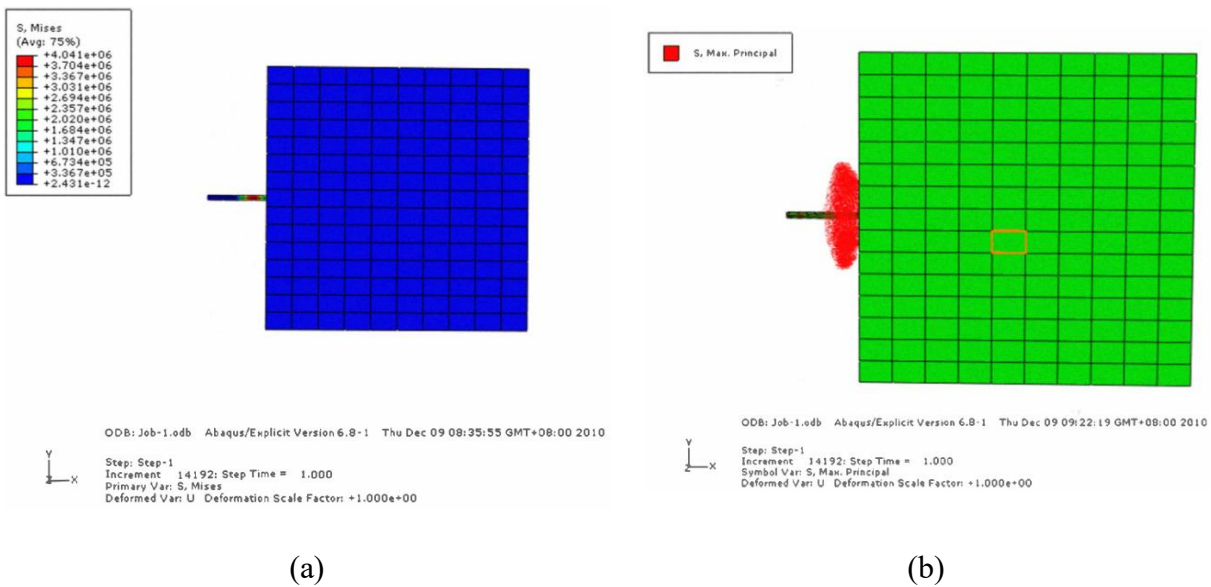(a)   (b)

Figure 20. Simulation of needle at the time of insertion in tissue, (a) Maximum stress, (b) Maximum bending [39].

Misra et al. [40] conducted numerical simulations on a commercially available finite software ABAQUS of bevel-tip needle and tissue-needle interaction. Tissue properties were measured experimentally and was used in the simulation. For deflection of bevel tip needle, the deflection function equation of needle was considered. The equation used is as follows:

$$\rho = f\left(\underbrace{E, I, \alpha}_{needle}, \underbrace{C_{10}, G_c, \mu}_{tissue}, \underbrace{u}_{input}\right) \tag{10}$$

They observed that 38% variation in nonlinear material elasticity did not produce any significant changes in tip forces. Furthermore, smaller bevel angles resulted in larger axial and transverse tip forces. Yong-de Zhang et al. [39] additionally developed a physical model using ABAQUS. For the simulation, a high nickel-titanium wire was utilized. The simulation's outcome demonstrated that the

needle's maximal stress was produced when it was inserted into the tissue (Figure 20).

Goksel et al. [19] presented two simulation models. Geometry for deformations and a non-linear material model were taken into account in both models. Three-dimensional Euler-Bernoulli nonlinear beam elements were utilized in the second model, whereas a 4-node tetrahedral element was used in the first. Young's modulus characterizes the needle bending in both versions. Additionally, a 3D spring mass analytical approach was offered for the validation task. The analytical approach by Goksel et al. [19] is discussed in section 2.3. It was concluded, that overall beam element model was computationally more efficient and require a smaller number of elements than the tetrahedral elements.

Gao et al. [8] created a novel kind of simulation program for the insertion of a flexible needle into soft tissue. Axial and radial forces were taken into consideration for the simulation. Combining the cutting and friction forces results in an axial force, whereas the tissue force is represented by the virtual spring model in radial force.

3. Path and motion planning for flexible needle

Since the aim of a needle-based intervention is to avoid the anatomical obstacle through the patient, path planning is an essential component. The primary goal is to precisely achieve the target by inserting the needle at a location on the tissue, avoiding any blockades along the way. Numerous unknowns, such as target movability, tissue deformation and tissue inhomogeneity, exist in the path planning of needles. The path planning may also be impacted by the patient's breath.

When path planning, a number of elements are taken into account, including target coordinates, blood vessels, bones, sensitive tissues and the site of the needle insertion (based on ultrasound probes), imaging cameras etc. Path planning is computed using any kinematic approach, accounting for all the previously described factors. Path planning is the strategy or plan that a robot or surgeon uses to get to the intended result. However, active needle route design is generally advised due to the intricacy of the patient's anatomy. The brief summary of the developed path planning models is shown in Table 2.

To fulfill the primary goal of path planning various fundamental path planning algorithms are employed to control the needle's tip. These algorithms include Adaptive Path Planning, Random-Exploring Random Tree (RRT), modified forms of RRT, Adaptive Fracture Tree, Screw-Based Path Planning and Path of Probability [11,17,41-43]. Finding the precise injection point turns out to be the hardest part. An adaptive fracture tree path planning model has been devised for the purpose of actively controlling the needle and maneuvering around obstructions. Similar to RRT*, the Adaptive Fracture Tree (AFT) method optimizes the path to avoid obstacles by first generating every potential path between the initial and target points. On the other hand, the AFT algorithm functions in three discrete stages: Path identification, comprehensive assessment of potential collisions, reassessment of collision risks and ultimate implementation. In the majority of path planning algorithms, the term "duty cycle" is essential. Maximum curvature is attained when the duty cycle is 0, whereas a straight line is produced when the value is 1. At varying duty cycle values between zero and one, different needle curvatures are obtained. An extensive explanation of each path planning algorithm will be provided in the subsequent sections.

Table 2. Summary of path planning models.

Sr No.	Author	Basic model	Modification	with or without obstacle	2D/3D
1	Park et al. (2010) [32]	Stochastic non-holonomic model	Path of probability (POP) algorithm	2	—
2	Duindam et al. (2008) [33]	Webster non-holonomic model	stop-and-turn, helical strategies	2	3D
3	Y. J. Zhao et al. (2012) [8]	Kinematic model	Improved kinematic model (reverse path planning)	1	2D
4	Bernardes et al. (2013) [34]	Rapidly-Exploring Random Tree (RRT)	Arc-RRT	1	2D
5	Y. J. Zhao et al. (2014) [35]	Rapidly-Exploring Random Tree (RRT)	RGHG-RRTs algorithm	1	2D
6	Y. J. Zhao et al. (2016) [36]	RGHG-RRTs algorithm	RGHG-RRTs algorithm with replanning algorithm	1	3D
7	Li et al. (2017) [37]	Lie Algebra	Discrete potential	1	3D

0 =Without obstacle, 1 = With obstacle, 2 = With and without Obstacle

3.2. Open-loop and close-loop needle steering

A necessary component of open-loop needle steering is path planning. Following path planning, the needle is placed without receiving any feedback, as seen in Figure 21. In contrast, with a close-loop needle steering technique, needle direction is not restricted to path planning. Anatomical goals and impediments are not set in vivo tissues; rather, the needle can be guided in any desired direction by a surgeon or computer based on sensor feedback, as demonstrated in Figure 22. The advantage of the latter approach is active feedback control, which allows the needle to be changed right away if something goes wrong. To reduce the needle motion, uncertainties and sensor noises, a kinematic technique with LQG controller and Random-Exploring Random Tree (RRT) can also be utilized [44].
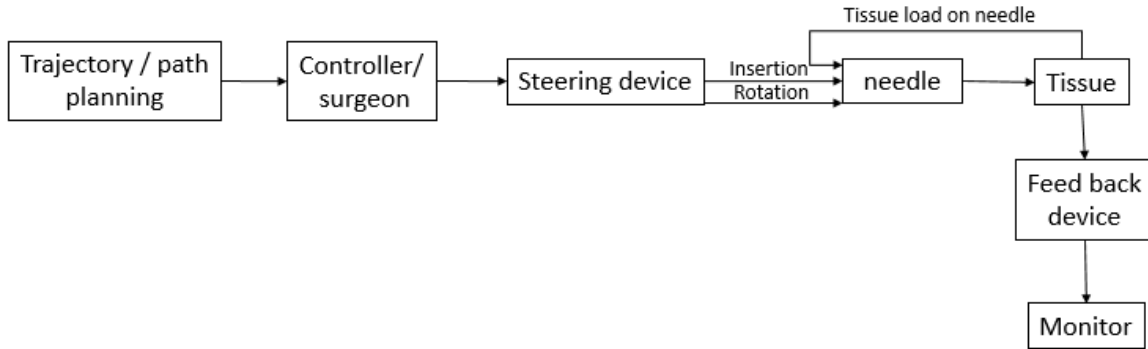
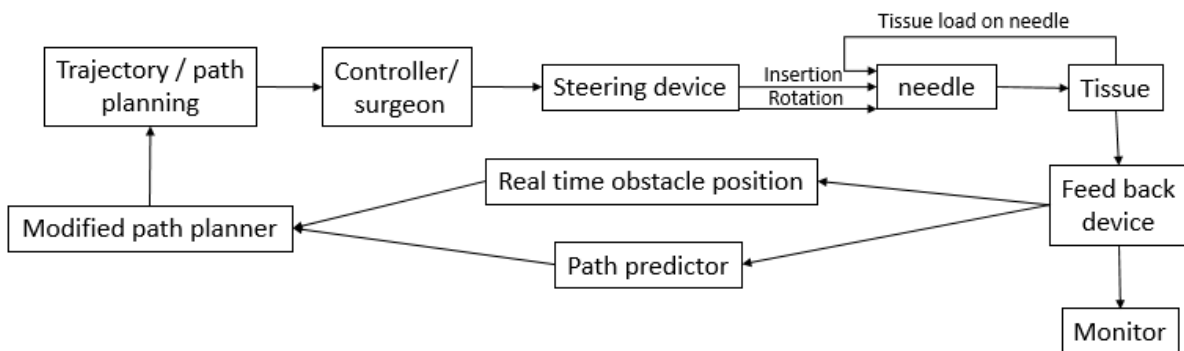**Figure 21.** Open-loop needle steering system.

Figure 22. Closed-loop needle steering system.

Bernardes et al. [41] developed a closed-loop adaptive image-guided automatic steering system for a bevel tip needle. The robot-assisted system actively guides the needle on the basis of information extracted from image feedback (Figure 23). The key benefits of this system that it can compensate for all uncertainties like needle tip error, needle modelling, inhomogeneity in tissue and change in obstacle or target due to patent movement [41].
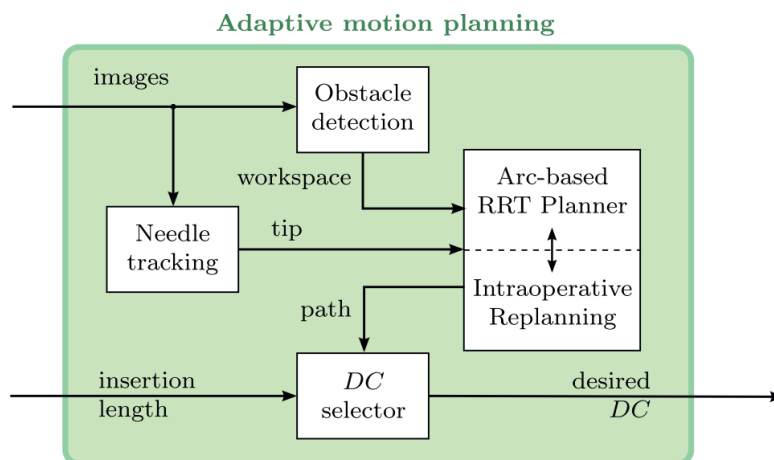

Figure 23. Flow chart of adaptive motion planning [41].

3.3. Random-exploring random tree

Duindam et al. [17] implemented the Random-Exploring Random Technique (RRT) to plan the flexible needle's path and motion and created a unidirectional exploration in the three-dimensional space. The flexible needle's entry point selection is a critical issue for motion planning. Moreover, the RRT structure can use a method that proved effective in C-space to overcome this entry point problem. Path planning also faces challenges from anatomical obstructions [17].

Anatomical obstacles can change its position as a result of patent motions, tissue softness and deformation inhomogeneity. The use of Arc-RRT active needle guiding can increase these uncertainties (Figure 24). As the needle travels through the tissue, the Arc-RRT continuously updates the planned path based on the workspace and current needle bevel tip position. The needle tip serves as the beginning point and moves toward the current target position with each insertion. The new function Get-ARC computes the new curvature and orientation based on these two current places and adjusts the needle arc from the beginning point, as indicated in Figure 24 [41].

RRT has been integrated with the Greedy Heuristic Strategy (GHS) and Reachability Guided Strategy (RGS) to accelerate the improvement in convergence at the target location. The algorithm, known by its acronym RGHG-RRTs, operated in two ways. The technique analyzes if a path may create directly or from starting to final node, including linear or curvilinear collision-free path in 2D environment, rather than generating the tree node instantaneously [45]. Zhao et al. [42] added the preplanning path in a 3D environment to their RGHG-RRTs model. Furthermore, three distinct preplanning techniques were provided to address issues with convergence and precision. They proposed OPTS (old point tracking strategy), ETES (extreme trend extension technique) and HGTS using the CMR, IMR-1 and IMR-2 algorithms (highly effective for convergence and accuracy problems) [42].
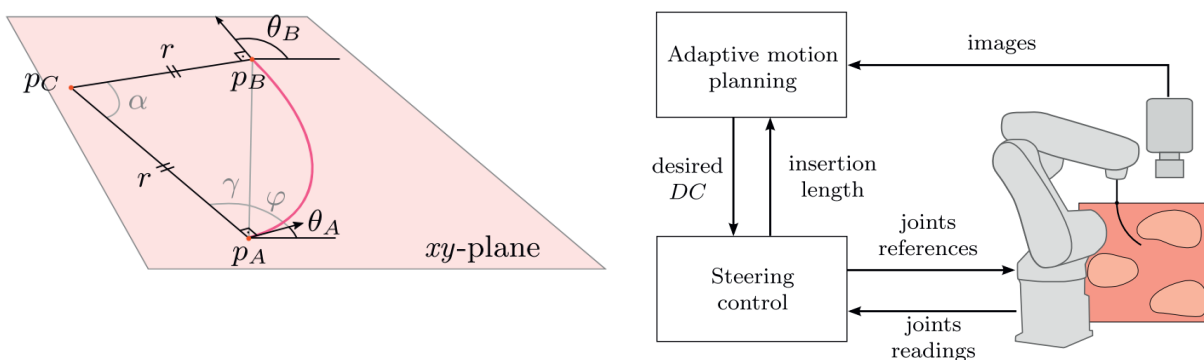

Figure 24. Arc-RRT active needle path planning technique [41].

3.4. Adaptive fractal tree

An active path planning technique that is comparable to RRT but somewhat quicker and more accurate is called Adoptive Fractal Tree (AFT). The three primary components of AFT path planning

are motion segment reconstruction, collision detection and target distance computation and backtracking and pooling.
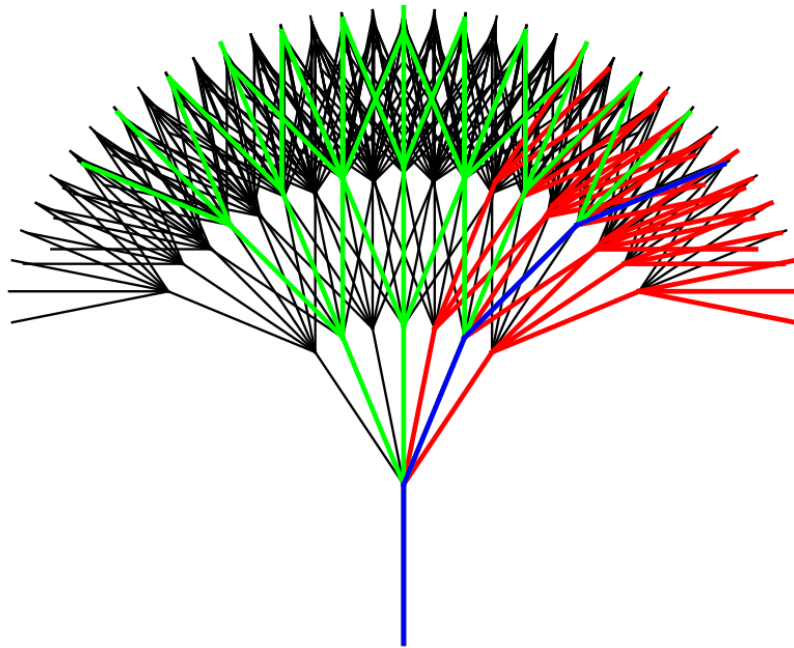

Figure 25. Illustration of the adaptive search concept; green tree explores the entire tree domain, red tree shows the most promising region and the blue tree shows the most suitable path [43].

A comprehensive database containing every path is created in the first section. Feedback sources like ultrasound and interventional magnetic resonance imaging initially presume the placement of all barriers, including the beginning point and goal point. Since most of the generated pathways have complex shapes, collision detection is applied to all of them in the second section. The AFT path planner determines which path segment has the highest probability of collisions with anatomical barriers. The method additionally calculates the target's distance from each segment's beginning. In the third section, AFT retraces every path to check for collision risks and marks or indicates every path that is clear and feasible (Figure 25) [43].

3.5. Screw-based 3D path planning and helical strategy

Duindam et al. [11] developed two different algorithms for 3D path planning. The algorithms were based on Webster [6] analytical model and work on two basic strategies, i.e. stop-and-turn strategy and helical strategy, as shown in Figure 26.
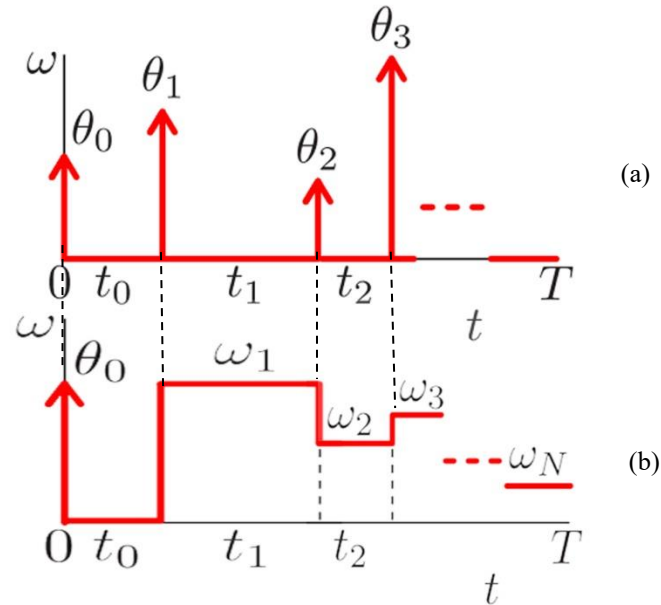
Figure 26. Two-path planning strategies with $\omega(t)$; (a) Stop-and-turn strategy, (b) Helical strategy [11].

Instead of using a helical strategy, the control in the stop and turn strategy alternates the needle's translation and angular velocity on a periodic basis. First, the needle is oriented at ($\omega \neq 0$, v = 0), then it is translated forward ($\omega = 0$, v $\neq 0$), at the time of reorientation ($\omega \neq 0$, v = 0), and so on (Figure 26b). However, in helical strategy, needle oriented at $\omega \neq 0$, v = 0), then it is translated forward ($\omega = 0$, v $\neq$ 0), at the time of reorientation ($\omega \neq 0$, v = 0), then translate and rotate at the same time ($\omega \neq 0$, v $\neq 0$), reorientation ($\omega \neq 0$, v = 0), again translate and rotate ($\omega \neq 0$, v $\neq 0$). That is the main reason helical strategy enhances a cost function, but discretize $\omega(t)$ to be a piecewise constant function (Figure 26a).

In the result of these two strategies, optimal trajectories have been developed in obstacle free environment which is shown in Figure 27. In obstacle free motion planning, the goal positions set in a grid with (0, -3, 10) and (0, 3, 10). The initial angle θ_0 and time t_0, and next angle θ_1 when using stop-turn strategy and angular velocity for helical strategy and time duration t_1 and so on. Figure 27 shows that, stop-turn strategy has maximum constant cost around 0.002 for all the goal positions, in contrast helical strategy has more variable cost depending on the position of the goal and maximum coast of around 0.9 at the position for (0, 0, 10), which is vertical position from initial position. Moreover, helical strategy fails to reach the vertical position goals [11]. Due to these two factors, stop-turn strategy is more useful than helical strategy in a given environment.
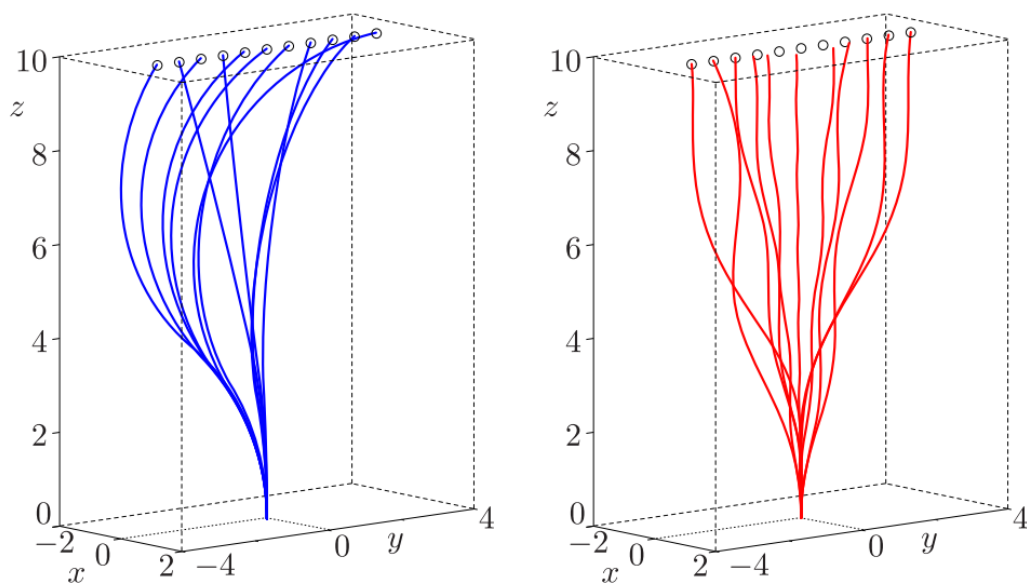
(a) Stop-and-turn strategy, $x_g = 0$.

(b) Helical strategy, $x_g = 0$.
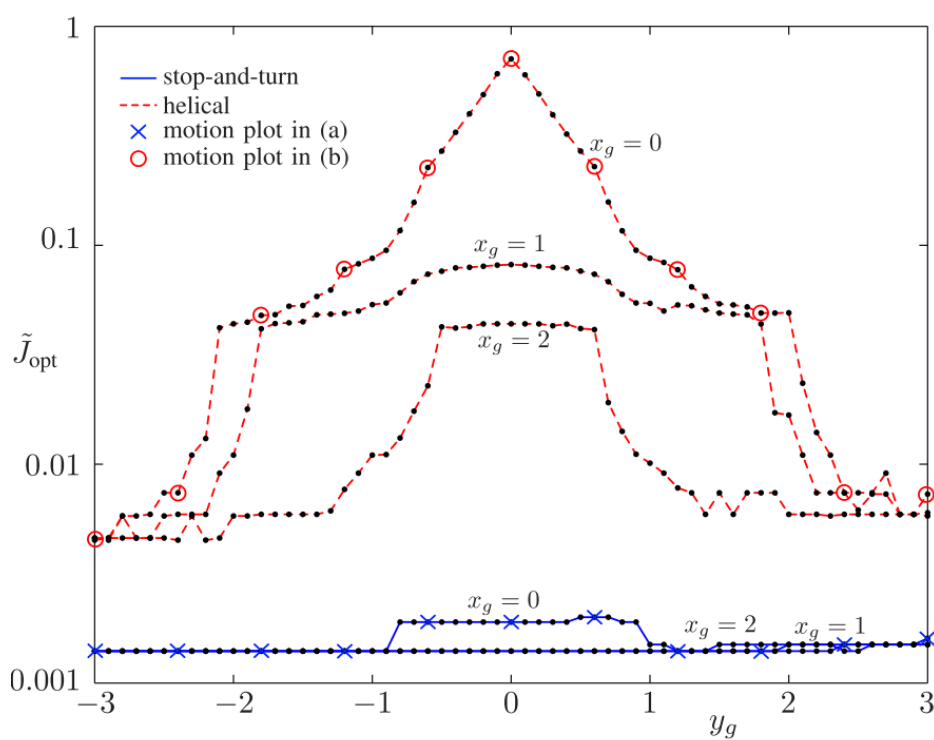
(c) Cost $\tilde{J}_{\text{opt}}$ associated with the optimal motions.

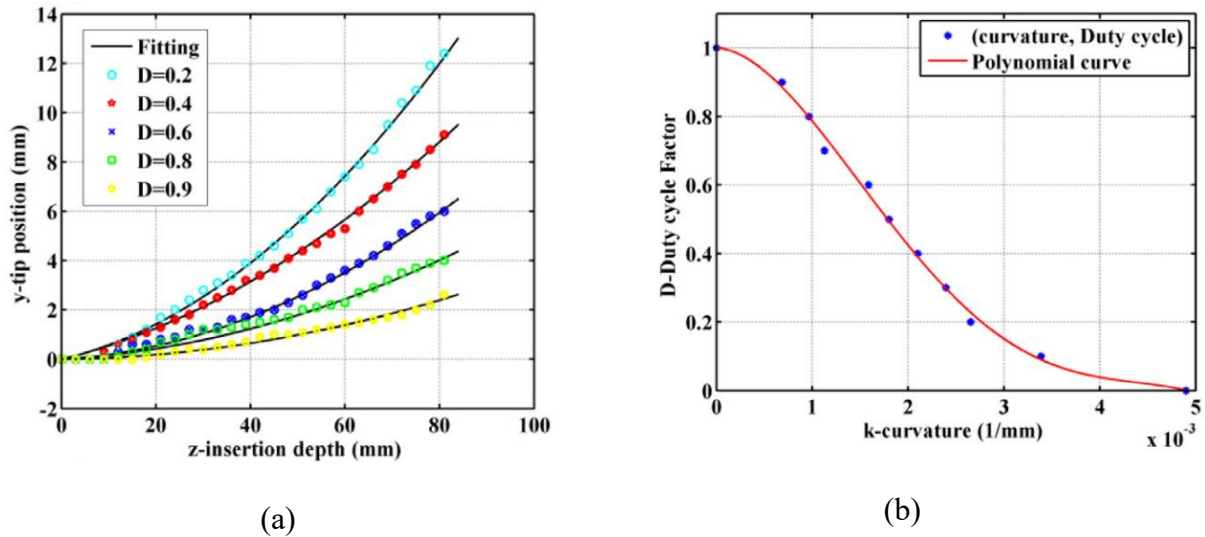**Figure 27**. Results in obstacle free environment for different positions [11].

(a)   (b)

Figure 28. Trajectories FN tip needle with different DCF. (a) Trajectories in y-direction. (b) relationship between curvature and DCE [46].
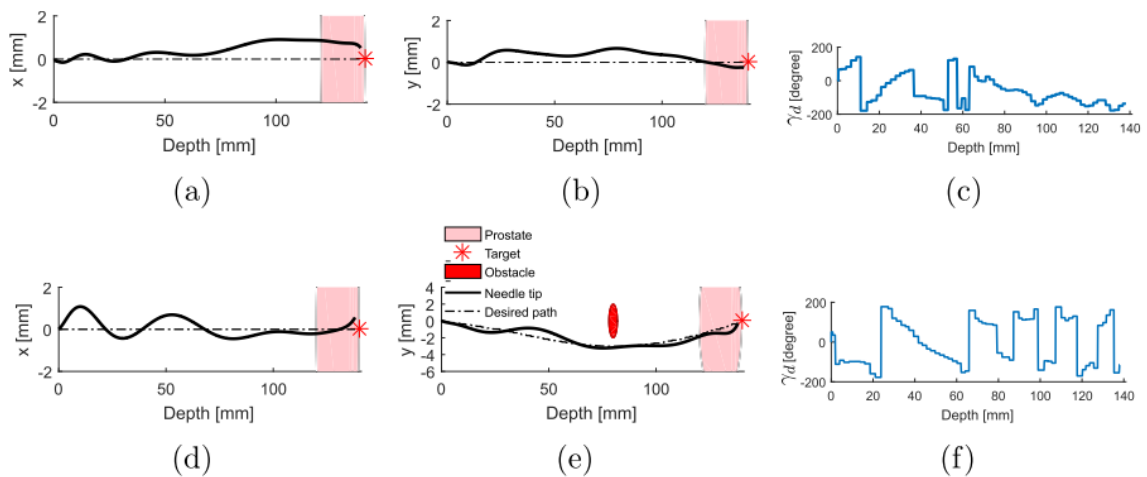
.

(a)   (b)   (c)

(d)   (e)   (f)

Figure 29. Needle insertion into phantom tissue; (a), (b), (c) without obstacle in x and y direction with rotation angle information; (d), (e), (f) with obstacle in x and y direction with rotation angle information [47].

Li et al. [46] found the relationship between helical strategy with duty-cycle. The study showed that as Duty Cycle Factor (DCF) increases needle tip deflection in y-axis decreases. From the Figure 28, it can be seen that the curvature will be zero at 1-DCF and maximum at 0-DCF [46].

Fallahi et al. [47] used two sliding surfaces in the x and y directions and a stop-turn strategy to reduce the chance of needle tip deflection errors when the needle is inserted and moves through the tissue in a z-direction (depth direction). The slides were equipped with an ultrasonic probe to enable real-time tracking of the needle's location. The controller rotated the needle to align it with the required position based on these coordinates, as shown in Figure 29.

3.6. Path of probability (POP)

Park et al. [48] suggested a new path planning model for the flexible needle employing the Probability Density Function in closed form and the Path of Probability (POP) algorithm (PDF). The model was derived from a stochastic needle steering model in which the needle tip's PDF is roughly Gaussian. The flexible needle stochastic model with bevel tips served as the model for the POP algorithm. The authors referred to the addition of all uncertainty in the control inputs as "white noise." [48]. The noise term was added as following equation:

$$\omega(t) = \omega_o(t) + \lambda w(t) \tag{11}$$

Here, λ is the noise parameter and $\omega(t)$ is the gaussian white noise.
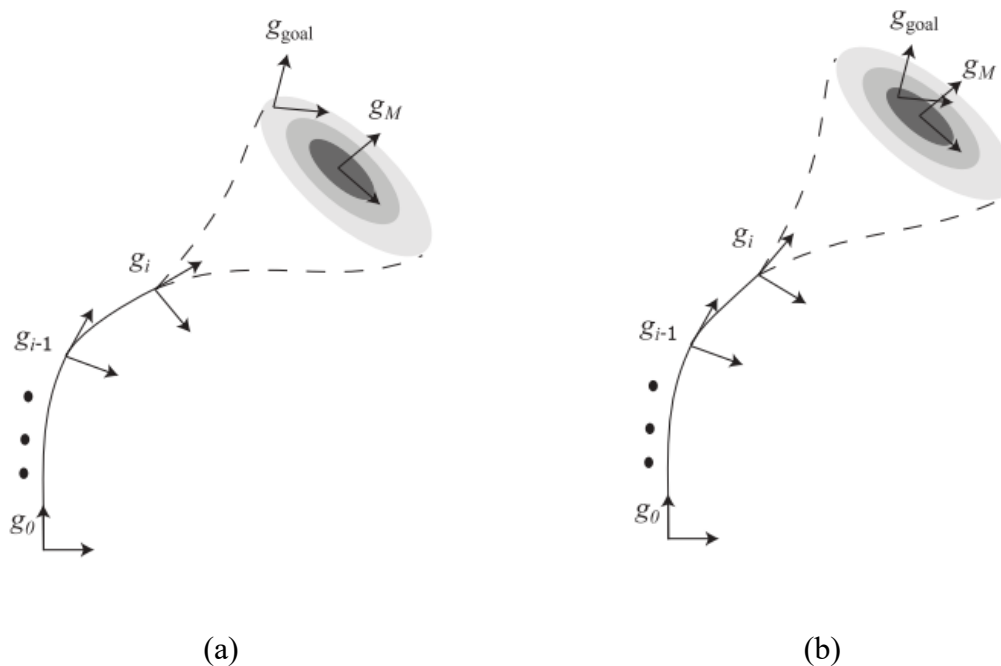

Figure 30. POP algorithm with intermediate steps, (a) Algorithm with a low probability of reaching the target. (b) Algorithm with a high probability of reaching the target [48].

The POP algorithm examines several different intermediate paths to reach the target (Figure 30). The path starts at g_o and finish at g_{goal} using several intermediate steps. The colored circle in Figure 30 shows the probability density function with all intermediate stages (M − i) taken into account, where M is the total number of steps. If all intermediate steps are considered after g_o, the needle will reach at the darkest area which has high accuracy. The authors went on to say that in a straightforward scenario with no blockades, the insertion site and orientation can be freely chosen and the POP algorithm will supply the needle path. The model's simulation also showed that the path planning technique is effective in the presence of intermediate insertion errors. The authors proposed that, even though the POP method was intended to operate in an obstacle-free environment, the model might be made to function in an obstacle-filled environment by utilizing splines in conjunction with the algorithm [48].

3.7. 2D motion planning algorithm

For the first time, Y. J. Zhao et al. [2] introduced a reverse path planning methodology in a 2D environment. The strategy of reverse path planning is that, the path starts from the target, avoid obstacles and reach the entry point. This is due to the reason that optimization of the entry point is really difficult in forward path planning (Figure 31) [2]. Furthermore, the authors explained that in unicycle model error arises due to the flexibility of the tissue and the needle. The error depends on the type of connections like RR (arc-arc path), RL (arc-linear path) and LR (length-arc path), as shown in Figure 32. The compensation of these errors in the unicycle model can be made in the form of rebound parameters.
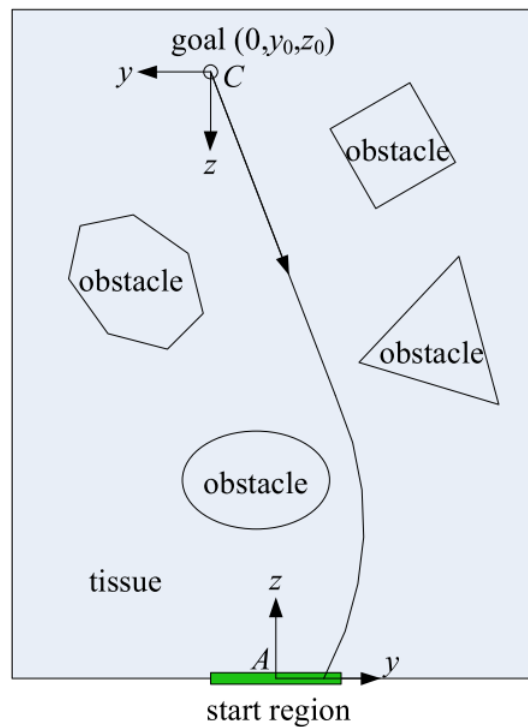

Figure 31. Optimization of entry point using reverse-path planning [2].

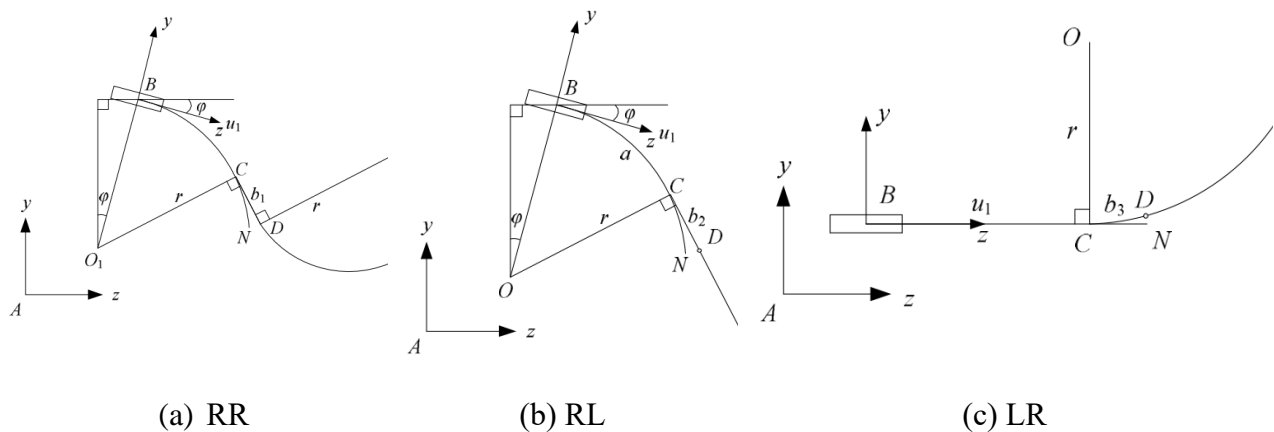

| (a) RR | (b) RL | (c) LR |

Figure 32. Rebounds experienced in different connections [2].

Zhang et al.[9] performed a path optimization research utilizing an enhanced unicycle kinematic model in a 2D environment with obstacles. They conducted experiments to validate their model. The optimized path from the carried-out study is superior to the RRT-based path, the scientists determined.
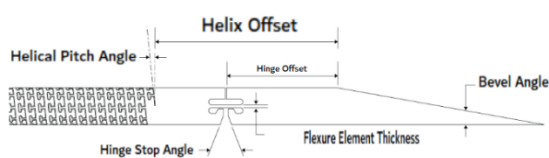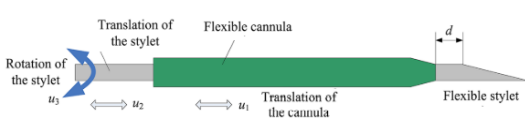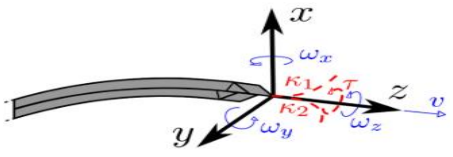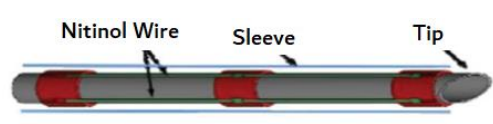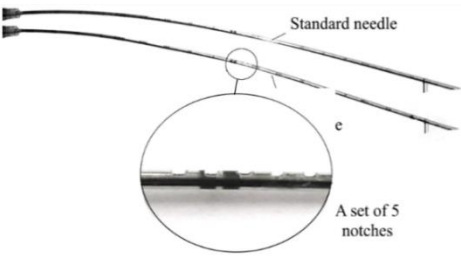
4. Needle types and controllers

Following the development of an accurate needle-tissue interaction model for predicting the position of bevel-tip type needles and the formulation of a path planning strategy, ensuring a reliable steering actuation technique is crucial to minimize targeting errors. Steering controllers, both active and passive, have been designed and implemented based on steering strategies. Passive steering relies on forces generated by needle-tissue interaction, while active steering involves additional efforts to enhance steering capabilities. Most bevel-tip needles employ a passive steering configuration, whereas active needles, as presented in Table 3, exhibit diverse designs and typically necessitate additional force applied to the needle tip through various actuators. Active needles effectively prevent targeting errors by allowing controlled bending of the needle tip. Although active needles tend to have symmetric tips, ensuring a straight trajectory with minimal effort [49], they are somewhat more accurate. However, their operational complexity increases due to additional control variables, making the system challenging to operate. Additionally, the larger size of active needles compared to asymmetric bevel needles can lead to increased tissue damage.

A robot designed for needle driving is commonly employed to control the insertion and rotation of the needle during precision testing operations. In some cases, the cannula is controllable and part of the needle steering mechanism. A robust driving mechanism is crucial since manual inputs alone may not adequately control rotation angle and insertion velocity.

Researchers have explored various steering techniques for flexible needles, as detailed in a comprehensive study by Mingyue Lu et al. [49]. According to their findings, trials demonstrated a 40% targeting inaccuracy, validated on artificial phantom tissue (76%), ex-vivo tissue (22%) and in-vivo biological tissue (2%). Passive needles are driven by the insertion and rotation of the needle base. In a study by Van de Berg et al. [50], various active needle designs and their mechanisms were discussed, encompassing bevel-tip type, active cannula, pre-curved style, tendon-actuated and programmable needle steering. Table 3 provides an overview of the designed and adopted needle types by researchers and subsequent sections will delve into the details of needle design and control systems.

Table 3. Design choices between various needle types.

Author	Design	Country	Year	Needle
Margaret Rox et al. [50]	Helical dovetail laser patterning	USA	2020	
Zahra K. Varnamkhasti et al. [51]	wire-driven 3D steerable needle	USA	2020	
Yan-Jiang Zhao et al. [42][26]	Cannula flexible needle	China	2016, 2019	
Fan Yang et al. [52]	Fracture-directed steerable Needle	USA	2019	
Thomas Watts et al. [53][32]	Programmable bevel-tip needle	UK	2011, 2019	
M. Scali et al. [54]	Self- propelling bio-inspired needle	Netherlands	2019	
Felix Orlando Maria Joseph et al. [55]	Shape memory alloy actuated active flexible needle	USA	2018	
Mohsen Khadem et al. [56]	Notched steerable needles	Canada	2016, 2017	

Author	Design	Country	Year	Needle
Giada Gerboni et al. [57]	Bevel needle with bent section	USA	2017	
Alexander Leibinger et al. [58]	Biologically inspired four-part needle	UK	2016	
Nick J. van de Berg et al. [59]	Tendon actuation and FBG-based shape sensing	Netherlands	2015	
Riccardo Secoli et al. [60]	Programmable bevel	UK	2013	
Libo Tang, Yonghua Chen et al. [61]	Magnetic force aided compliant needle	HK	2007	

4.2. Passive needle steering controller

Webster et al. [62] two distinct robotic steering devices, each capable of controlling both rotation and translational velocity. The first device utilizes a friction drive mechanism, founded on the friction drive concept, as illustrated in Figure 33(a). The second device employs a telescoping mechanism, utilizing telescoping equipment support to prevent buckling, as depicted in Figure 33(b) [62].
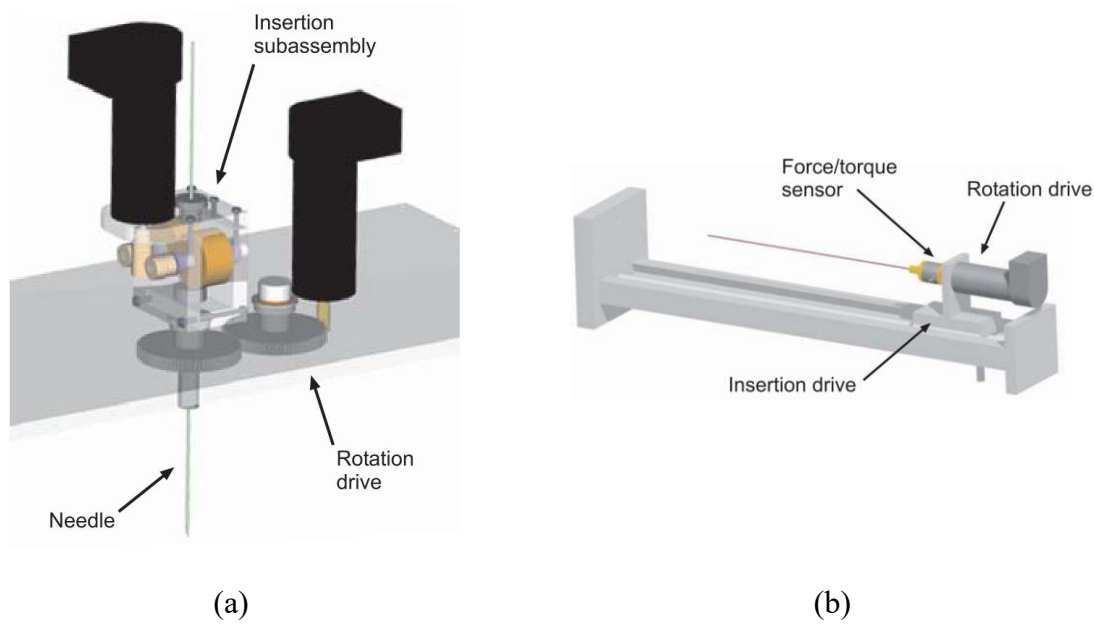
(a) (b)

Figure 33. CAD model of steering devices, (a) Friction drive device, (b) Telescoping support device [62].
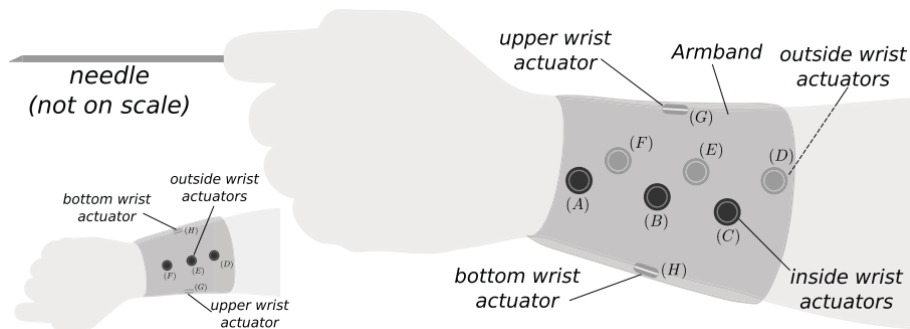

Figure 34. Rossa's haptic feedback wristband controller for needle steering [63].

Rossa el al. [63] developed a haptic feedback device worn on the wrist designed to guide needle steering in brachytherapy, as depicted in Figure 34. The wristband incorporates eight small actuators distributed around the wrist. These actuators produce various haptic stimuli, providing the surgeon with feedback to guide accurate and precise needle movements. Rossa el al. [3,4] also introduced a compact and user-friendly device with surgeon involvement. Their proposed system leverages ultrasound images and a needle-tissue interaction model to accurately predict the needle tip position in the tissue and the needle deflection during insertion. The needle steering algorithm gauges the needle depth at which rotation is necessary. Based on this information, the controller device rotates the needle to the desired depth and angle. The device is also capable of minimizing friction between the needle shaft and tissue by generating vibrations, facilitating smoother insertion. The cross-section of the device is illustrated in Figure 35. Subsequently, Carriere et al. [64] modified the device, by incorporating an event-trigger mechanism to reduce needle deflection during insertion.
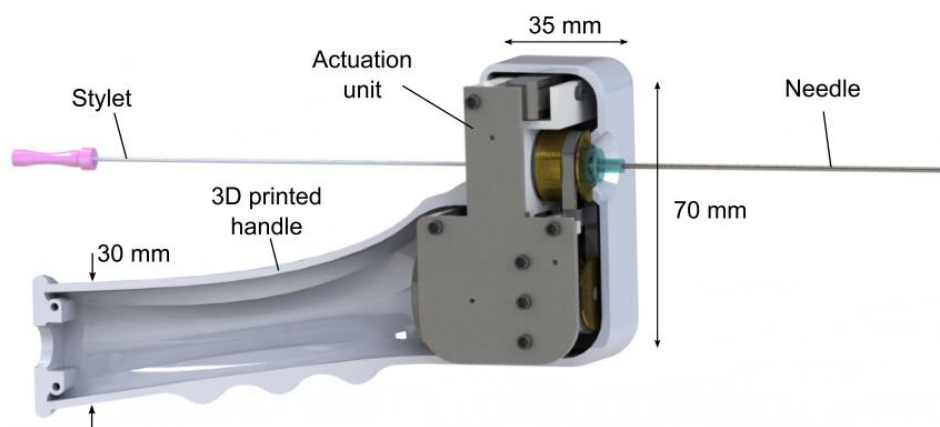
Figure 35. Hand-held needle steering assistant [3].

4.3. Mechanization level of controllers

Table 4. Controller with their automation level.

Sr No.	Author	Controller	Automation level	Device Actuator
1	Webster et al. (2005) [41]	Friction drive device	A	2
		Telescoping support device	A	2
2	Rossa et al. (2016) [42]	Haptic Wristband	S	0
3	Rossa et al. (2016) [43]	The Hand -held Assistant	S	1
4	Asadian et al. (2011) [44]	Robotic system	A	2
5	Rossa et al. (2016) [12]	Robotic system	A	2
6	Lehmann et al. (2017) [19]	Hand-held needle steering assistant (HNSA)	S	3
7	Yong-de Zhang et al. (2011) [45]	Needle insertion mechanism	A	2
8	Khadem Mohsen (2019) [16]	Two-step controller	M	1

Aautomation level: Surgeon in loop (S), Fully Automated (A), Manual (M); Device actuator: Only Guidance (0), Only Rotation (1), Rotation + Translation (2), Rotation + Lateral force (3)

In order to facilitate needle guidance during procedures like seed implantation or biopsy, sophisticated needle steering devices and controls have been developed. These systems can be broadly categorized based on the level of automation in the steering control system, dividing them into three categories: totally manual, semi-automated and automated insertion. In automated systems, robots execute the entire needle insertion process. In semi-automated systems, robotic control handles

translation, but the surgeon or physician controls the insertion. The third category involves the device providing information on the needle's position, with the surgeon or physician manually regulating rotation and translation movements. Table **4** outlines the types of controllers, their degree of automation and their flexibility levels.

5. Conclusions

In this paper, we present a detailed review of recent developments in the field of tissue-needle interaction and flexible needle path planning. Various crucial aspects of flexible needle design and implementation for soft tissue interventions are explored. These considerations encompass the needle-tissue interaction model, validation through numerical techniques, path planning development and the design of robotic actuators for controlling needle insertion and angle.

The review highlights the comparison and detailed discussion of various models, including non-holonomic, mechanics-based, virtual spring-based, stochastic and Finite Element Analysis (FEA)-based mathematical models. It was observed that mechanics-based models are more reliable, demonstrating higher accuracy and reliability in tissue interactions, while the uni-cycle model exhibits the maximum error among various models. The inclusion of schematic diagrams facilitates easy classification and relevance of models, indicating whether they are validated through experimentation, simulation or both, and in what environment (2D/3D, with or without obstacles). We also address simulation, path planning and explore different needle types and controlling mechanisms.

For future work, a comprehensive study could delve into path planning with schematic comparisons presented in a table format. Additionally, further exploration of the materials used for manufacturing needles and tissue could enhance the depth of understanding in this field.

Use of AI tools declaration

The authors declare they have not used Artificial Intelligence (AI) tools in the creation of this article.

Conflict of interest

The authors have no conflict of interest, financial or otherwise.

Funding

References

1. R. Alterovitz, M. Branicky, K. Goldberg, Motion planning under uncertainty for image-guided medical needle steering, *Int. J. Rob Res.*, **27** (2008), 1361–1374. https://doi.org/10.1177/0278364908097661
2. Y. J. Zhao, Y. D. Zhang, F. Tu, Reverse path planning for flexible needle in 2D soft tissue with

obstacles, *Appl. Mech. Mater.*, **121**-**126** (2012), 4132–4137. https://doi.org/10.4028/www.scientific.net/AMM.121-126.4132

3.   C. Rossa, N. Usmani, R. Sloboda, A hand-held assistant for semiautomated percutaneous needle steering, *IEEE Trans. Biomed Eng.*, **64** (2017), 637–648. https://doi.org/10.1109/TBME.2016.2565690

4.   C. Rossa, M Tavakoli, Issues in closed-loop needle steering, *Control Eng. Pract.*, **62** (2017), 55–69. https://doi.org/10.1016/j.conengprac.2017.03.004

5.   W. Park, J. S. Kim, Y. Zhou, Diffusion-based motion planning for a nonholonomic flexible needle model, in *Proceedings of the IEEE Int. Conf. Robot Automation*, (2005), 1050–4729. https://doi.org/10.1109/ROBOT.2005.1570829

6.   R. J. Webster, J. S.Kin, N. J. Cowan, G. S. Chirikjian, A. M. Okamura, Nonholonomic modeling of needle steering, *Tract.s Adv. Robot.*, **21** (2006), 35–44. https://doi.org/10.1177/0278364906065388

7.   S. Misra, K. T. Ramesh, A. M. Okamura, Modeling of tool-tissue interactions for computer-based surgical simulation: A lit review, *Teleoper. Virt. Env.*, **17** (2008), 463–491. https://doi.org/10.1162/pres.17.5.463

8.   D. Gao, Y. Lei, B. Lian, Modeling and Simulation of Flexible Needle Insertion into Soft Tissue Using Modified Local Constraints, *J. Manuf. Sci. Eng. ASME*, **138** (2016), 1–10. https://doi.org/10.1115/1.4034134

9.   T. D. Zhang, K. M. Shi, Y. J. Zhao, J. C. Yang, J. Liu, Path optimization algorithm and its robustness for bevel tip flexible needle, *Int. J. Adv. Robot Syst.*, **15** (2018), 1–11. https://doi.org/10.1177/1729881418801166

10. D. Glozman, M. Shoham, Flexible needle steering and optimal trajectory planning for percutaneous therapies, *Int. Conf. Med. Image Computer-assisted Intervent.*, **3217** (2004), 137–144. https://doi.org/10.1007/978-3-540-30136-3_18

11. V. Duindam, R. Alterovitz, S. Sastry, K. Goldberg, Screw-based motion planning for bevel-tip flexible needles in 3D environments with obstacles, in *Proc. - IEEE Int. Conf. Robot Autom.*, **22146911** (2008), 2483–2488. https://doi.org/10.1109%2FROBOT.2008.4543586

12. R. Secoli, F. R. Y. Baena, Adaptive path-following control for bio-inspired steerable needles, in *Proc. IEEE RAS EMBS Int. Conf. Biomed. Robot. Biomechatron.*, (2016), 87–93. https://doi.org/10.1109/BIOROB.2016.7523603

13. R. Sun, T. Yang, Hybrid parameter-based PSO flexible needle percutaneous puncture path planning, *J. Supercomput.*, (2023), 1–20. https://doi.org/10.1007/s11227-023-05661-x

14. Z. Tan, D. Zhang, H. G. Liang, Q. G. Wang, W. Cai, A new path planning method for bevel-tip flexible needle insertion in 3D space with multiple targets and obstacles, *Control Theory Technol.*, **20** (2022), 525–535. https://doi.org/10.1007/s11768-022-00113-y

15. A. Segato, F. Calimeri, I. Testa, V. Corbetta, M. Riva, E. D. Momi, A hybrid inductive learning-based and deductive reasoning-based 3-D path planning method in complex environments, *Auton. Robots*, **46** (2022), 645–666. https://doi.org/10.1007/s10514-022-10042-z

16. Z. Li, J. Dankelman,E. D. Momi, Path planning for endovascular catheterization under curvature constraints via two-phase searching approach, *Int. J. Comput. Assist. Radiol. Surg.*, **16** (2021), 619–627. https://doi.org/10.1007/s11548-021-02328-x

17. J. Xue, V. Duindam, R. Alterovitz, K. Goldberg, Motion planning for steerable needles in 3D environments with obstacles using Rapidly-exploring random trees and backchaining, in *4th IEEE Conf. Autom. Sci. Eng. CASE*, (2008), 41–46. https://doi.org/10.1109/COASE.2008.4626486

18. K. G. Yan, T. Podder, Y. Yu, T. Liu, C. W. Cheng, Flexible needle-tissue interaction modeling with depth-varying mean parameter: Preliminary study, *IEEE Trans. Biomed. Eng.*, **56** (2009), 255–262. https://doi.org/10.1109/tbme.2008.2005959

19. O. Goksel, E. Dehghan, S. E. Salcudean, Modeling and simulation of flexible needles, *Med. Eng. Phys.*, **31** (2009), 1069–1078. https://doi.org/10.1016/j.medengphy.2009.07.007

20. A. Asadian, M. R. Kermani, R. V. Patel, An analytical model for deflection of flexible needles during needle insertion, *IEEE. Int. Conf. Intell. Robot. Syst.*, (2011), 2551–2556. https://doi.org/10.1109/IROS.2011.6094959

21. C. Rossa, R. Sloboda, N. Usmani, Estimating needle tip deflection in biological tissue from a single transverse ultrasound image: Application to brachytherapy, *Int. J. Comput. Assist. Radiol. Surg.*, **11** (2016), 1347–1359. https://doi.org/10.1007/s11548-015-1329-4

22. X. Zhao, L. Kong, D. Ye, Y. Zhao, Z. Wu, Flexible tip-steerable needle control with tissue uncertainty, in *26th Chinese Control Decis. Conf. CCDC*, (2014), 4612–4616. https://doi.org/10.1109/CCDC.2014.6852996

23. M. Khadem, C. Rossa, N. Usmani, R. S. Sloboda, M. Tavakoli, Semi-Automated Needle Steering in Biological Tissue Using an Ultrasound-Based Deflection Predictor, *Ann. Biomed. Eng.*, **45** (2017), 924–938. https://doi.org/10.1007/s10439-016-1736-x

24. M, Khadem, C. Rossa, N. Usmani, R. S. Sloboda, M. Tavakoli, Feedback-linearization-based 3D needle steering in a Frenet-Serret frame using a reduced order bicycle model, *Proc. Am. Control Conf.*, (2017), 1438–1443. https://doi.org/10.23919/ACC.2017.7963155

25. M. Khadem, C. Rossa, N. Usmani, R. S. Sloboda, M. Tavakoli, Geometric control of 3D needle steering in soft-tissue, *Automatica*, **101** (2019), 36–43. https://doi.org/10.1016/j.automatica.2018.11.018

26. Y. Zhao, Z. Liu, Y. D. Zhang, Z. Q. Liu, Kinematic model and its parameter identification for cannula flexible needle insertion into soft tissue, *Adv. Mech. Eng.*, **11** (2019), 1–13. https://doi.org/10.1177/1687814019852185

27. S. Misra, K. B. Reed, B. W. Schafer, K. T. Ramesh, A. M. Okamura, Mechanics of Flexible Needles Robotically Steered through Soft Tissue, *Int. J. Rob. Res.*, **29** (2010), 1640–1660 https://doi.org/10.1177/0278364910369714

28. R. J. Roesthuis, M. Abayazid, S. Misra, Mechanics-based model for predicting in-plane needle deflection with multiple bends, in *Proc. IEEE RAS EMBS Int. Conf. Biomed. Robot Biomechatron.*, (2012), 69–74. https://doi.org/10.1109/BioRob.2012.6290829

29. M. Khadem, B. Fallahi, C. Rossa, R. S. Sloboda, N. Usmani, M. Tavakoli, A mechanics-based model for simulation and control of flexible needle insertion in soft tissue, in *Proc - IEEE Int. Conf. Robot. Autom.*, (2015), 2264–2269. https://doi.org/10.1109/ICRA.2015.7139499

30. C. Rossa, M. Khadem, R. Sloboda, N. Usmani, M. Tavakoli, Adaptive Quasi-Static Modelling of Needle Deflection during Steering in Soft Tissue, *IEEE. Robot. Autom. Lett.*, **1** (2016), 916–923. https://doi.org/10.1109/LRA.2016.2527065

31. T. Lehmann, C. Rossa, N. Usmani, R. Sloboda, M. Tavakoli, Deflection modeling for a needle

actuated by lateral force and axial rotation during insertion in soft phantom tissue, *Mechatronics*, **48** (2017), 42–53. https://doi.org/10.1016/j.mechatronics.2017.10.008

32. T. Watts, R. Secoli, F. R. Y. Baena, A Mechanics-Based Model for 3-D Steering of Programmable Bevel-Tip Needles, *IEEE Trans. Robot.*, **35** (2019), 371–386. https://doi.org/10.1109/TRO.2018.2879584

33. D. Glozman, M. Shoham, Image-Guided Robotic Flexible Needle Steering, *IEEE Trans. Robot.*, **23** (2007), 57–62. https://doi.org/10.1109/TRO.2007.898972

34. N. Sadati, M. Torabi, R. Vaziri, R. D. Ardekani, Soft-tissue modeling and image-guided control of steerable needles, in *Proc. 31st Annu. Int. Conf. IEEE Eng. Med. Biol. Sci. Eng. Futur. Biomed. EMBC*, (2009), 5122–5125. https://doi.org/10.1109/iembs.2009.5333473

35. W. park, Y. Liu, Y. Zhou, M. Moses, G. S. Chirikjian, Kinematic state estimation and motion planning for stochastic nonholonomic systems using the exponential map, *Robotica*, **26** (2008), 419–434. https://doi.org/10.1017/S0263574708004475

36. R. Taschereau, J. Pouliot, J. Roy, D. Tremblay, Seed misplacement and stabilizing needles in transperineal permanent prostate implants, *Radiother Oncol.*, **55** (2000), 59–63. https://doi.org/10.1016/s0167-8140(00)00162-6

37. R. Alterovitz, K. Goldberg, A. Okamura, Planning for steerable bevel-tip needle insertion through 2D soft tissue with obstacles, in *Proc. - IEEE Int. Conf. Robot. Autom.*, (2005), 1640–1645. https://doi.org/10.1109/ROBOT.2005.1570348

38. R. Alterovitz, K. Y. Goldberg, J. Pouliot, I. J. Hsu, Sensorless motion planning for medical needle insertion in deformable tissues, *IEEE. Trans. Inf. Technol. Biomed.*, **13** (2009), 217–225. https://doi.org/10.1109/titb.2008.2008393

39. Y. D. Zhang, F. Tu, The physical modeling of flexible needle biopsy soft tissue based on ABAQUS software, in *2011 IEEE/ICME Int. Conf. Complex. Med. Eng.*, (2011), 426–430. https://doi.org/10.1109/ICCME.2011.5876777

40. S. Misra, K. B. Reed, A. S. Douglas, K. T. Ramesh, A. M. Okamura, Needle-tissue interaction forces for bevel-tip steerable needles, in *Proc 2nd Bienn IEEE/RAS-EMBS Int, Conf, Biomed. Robot. Biomechatronics*, (2008), 224–231. https://doi.org/10.1109%2FBIOROB.2008.4762872

41. M. C. Bernardes, B. V. Adorno, P. Poignet, G. A. Borges, Robot-assisted automatic insertion of steerable needles with closed-loop imaging feedback and intraoperative trajectory replanning, *Mechatronics*, **23** (2013), 630–645. https://doi.org/10.1016/j.mechatronics.2013.06.004

42. Y. J. Zhao, W. Q. Wu, Y. D. Zhang, R. X. Wang, J. C. Peng, Y. Yu, 3D dynamic motion planning for robot-assisted cannula flexible needle insertion into soft tissue, *Int. J. Adv. Robot. Syst.*, **13** (2016), 1–11. https://doi.org/10.5772/64199

43. F. Liu, A. Garriga-Casanovas, R. Secoli, F. R. Y. Baena, Fast and adaptive fractal tree-based path planning for programmable bevel tip steerable needles, *IEEE. Robot. Autom. Lett.*, **1** (2016), 601–608. https://doi.org/10.1109/LRA.2016.2528292

44. J. Van Den Berg, S. Patil, R. Alterovitz, P. Abbeel, K. Goldberg, LQG-based planning, sensing, and control of steerable needles, *Springer Tracts. Adv. Robot.*, **68** (2010), 373–389. https://doi.org/10.1007/978-3-642-17452-0_22

45. Y. J. Zhao, F. O. M. Joseph, K. Yan, N. V. Datla, Y. D. Zhang, T. K. Podder, et al. Path planning for robot-assisted active flexible needle using improved Rapidly-Exploring Random trees, in *2014*

36th Annu. Int. Conf. IEEE Eng. Med. Biol. Soc. EMBC, (2014), 380–383. https://doi.org/10.1109/embc.2014.6943608

46. P. Li, S. Jiang, D. Liang, Z. Yang, Y. Yu, W. Wang, Modeling of path planning and needle steering with path tracking in anatomical soft tissues for minimally invasive surgery, *Med. Eng. Phys.*, **41** (2017), 35–45. https://doi.org/10.1016/j.medengphy.2017.01.006

47. B. Fallahi, C. Rossa, R. S. Sloboda, N. Usmani, M. Tavakoli, Sliding-based image-guided 3D needle steering in soft tissue, *Control. Eng. Pract.*, **63** (2017), 34–43. https://doi.org/10.1016/j.conengprac.2017.04.001

48. W. Park, Y. Wang, G. S. Chirikjian, The path-of-probability algorithm for steering and feedback control of flexible needles, *Int. J. Rob. Res.*, **29** (2010), 813–830. https://doi.org/10.1177/0278364909357228

49. M. Lu, Y. Zhang, C. M. Lim, H. Ren, Flexible needle steering with tethered and untethered actuation: Current states, targeting errors, challenges and opportunities, *Ann. Biomed. Eng.*, **51** (2023), 905–924. https://doi.org/10.1007/s10439-023-03163-8

50. M. Rox, M. Emerson, T. E. Ertop, I. Fried, M. Fu, J. Hoelscher, et al., Decoupling steerability from diameter: Helical dovetail laser patterning for steerable needles, *IEEE Explore*, **8** (2020), 181411–181419. https://doi.org/10.1109/ACCESS.2020.3028374

51. Z. K. Varnamkhasti, B. Konh, Compact 3D-printed active flexible needle for percutaneous procedures, *Surg. Innov.*, **27** (2020), 402–405. https://doi.org/10.1177/1553350620945564

52. F. Yang, M. Babaiasl, J. P. Swensen, Fracture-Directed Steerable Needles, *J. Med. Robot. Res.*, **4** (2019), 1842002. https://doi.org/10.1142/S2424905X18420023

53. S. Y. Ko, L. Frasson, Y. R. Y. Baena, Closed-loop planar motion control of a steerable probe with a programmable bevel inspired by nature, *IEEE Trans. Robot.*, **27** (2011), 970–983. https://doi.org/10.1109/TRO.2011.2159411

54. M. Scali, P. Breedveld, D. Dodou, Experimental evaluation of a self- propelling bio-inspired needle in single- and multi-layered phantoms, *Sci. Rep.*, (2019), 1–13. https://doi.org/10.1038/s41598-019-56403-0

55. F. O. M. Joseph, T. Podder, Sliding mode control of a shape memory alloy actuated active flexible needle, *Robotica*, **36** (2018), 1188–1205. http://dx.doi.org/10.1017/S0263574718000334

56. M. Khadem, C. Rossa, N. Usmani, R. S. Sloboda, M. Tavakoli, Robotic-Assisted Needle Steering Around Anatomical Obstacles Using Notched Steerable Needles, *IEEE J. Biomed. Heal. Informatics*, **22** (2017), 1917–1928. https://doi.org/10.1109/JBHI.2017.2780192

57. G. Gerboni, J. D. Greer, P. F. Laeseke, G. L. Hwang, A. M. Okamura, Highly articulated robotic needle achieves distributed ablation of liver tissue, *IEEE Explore*, **3766** (2017), 1–8. https://doi.org/10.1109%2FLRA.2017.2668467

58. A. Leibinger, M. J. Oldfield, F. R. Y. Baena, Minimally disruptive needle insertion: A biologically inspired solution, *Interface Focus*, **6** (2016), 1–10. https://doi.org/10.1098/rsfs.2015.0107

59. V. D. Berg, J. Dankelman, V. D. Dobbelsteen, Design of an actively controlled steerable needle with tendon actuation and FBG-based shape sensing, *Med. Eng. Phys.*, **37** (2015), 617–622. https://doi.org/10.1016/j.medengphy.2015.03.016

60. R. Secoli, F. R. Y. Baena, Closed-loop 3D motion modeling and control of a steerable needle for soft tissue surgery, in *Proc. - IEEE Int. Conf. Robot. Autom.*, (2013), 5831–5836.

https://doi.org/10.1109/ICRA.2013.6631416

61. L. Tang, Y. Chen, X He, Magnetic force aided compliant needle navigation and needle performance analysis, in *2007 IEEE Int. Conf. Robot. Biomimetics*, (2007), 612–616. https://doi.org/10.1109/ROBIO.2007.4522232

62. R. J. Webster, J. Memisevic, A. M. Okamura, Design considerations for needle steering, *Proc. IEEE Int. Conf. Robot. Autom.*, (2005), 3599–3605. https://doi.org/10.1109/ROBOT.2005.1570666

63. C. Rossa, J. Fong, N. Usmani, R. Sloboda, M. Tavakoli, Multiactuator Haptic Feedback on the Wrist for Needle Steering Guidance in Brachytherapy, *IEEE Robot. Autom. Lett.*, **1** (2016), 852–859. https://doi.org/10.1109/LRA.2016.2528295

64. J. Carriere, M. Khadem, C. Rossa, N. Usmani, R. Sloboda, M. Tavakoli, Event-Triggered 3D Needle Control Using a Reduced-Order Computationally Efficient Bicycle Model in a Constrained Optimization Framework, *J. Med. Robotics. Res.*, **4** (2019), 1–16. https://doi.org/10.1142/S2424905X18420047